Master of Science Thesis

Brachytherapy of Squamous Cell Carcinoma in the Lip: MDR to PDR Treatment Conversion

Daniel Gasic

Supervisor: Jens M. Edmund, PhD

The work has been performed at
Department of Oncology

Copenhagen University Hospital, Herlev, Denmark

Medical Radiation Physics
Clinical Sciences, Lund

Lund University, 2010

En behandlingsmetod som dödar tumören inifrån

En vanlig typ av behandling vid cancer är strålbehandling. Tekniken har utvecklats mycket de senaste åren och med ny teknik kommer bättre behandlingsresultat och bättre skydd mot strålningen. När det är dags att byta ut en äldre behandlingsteknik mot en nyare är det en del faktorer som måste undersökas. Detta arbete undersöker just de möjligheterna vid en ny typ av behandling för läppcancer.

Strålbehandling ges generellt sett med röntgenstrålning med hög energi vilket ger doser till omkringliggande vävnad. Genom att operera in den radioaktva källan i tumören så ökar bestrålningen till själva tumören samtidigt som den minskar till den friska vävnaden runtomkring.

Det finns radioaktiva källor som ser olika ut, är olika stora och avger olika mycket strålning. Arbetet undersöker möjligheten att byta ut en äldre typ av behandling, där läppcancer behandlades med radioaktiva iridiumtrådar mot den nyare, där behandlingen görs med en liten radioaktiv iridiumpellet som rör sig fram och tillbaka i tumören genom en nål och stannar på olika förbestämda positioner. Dessa förbestämda positioner kallas för stoppositioner. Ju kortare tid som pelleten stannar i en position desto mindre strålning når den omkringliggande vävnaden. Anledningen till behandlingsbytet är i första hand bättre skydd för personalen som arbetar med strålningen.

Genom att mäta hur strålningen utbreder sig från den radioaktiva källans mittpunkt med hjälp av en speciell självframkallande film, kan en bild av hur det ser ut målas upp. En bild över dosfördelningen från källan erhålls. Om detta görs för både den radioaktiva tråden och för den radioaktiva pelleten kan en jämförelse mellan dessa erhållas. Den lilla pelleten som är 3.6 mm lång avger mycket mer strålning än tråden som är 36 mm lång under samma tid, vilket betyder att strålningens spridning kommer att se olika ut för de båda källorna.

Flera jämförelser gjordes för tre olika avstånd från den radioaktiva källan. Resultaten visar att det finns en viss skillnad i dosfördelning mellan tråden och pelleten och därmed måste en kompensation göras för att minska skillnaden. Skillnaden är som minst när de bägge källorna är placerade i mitten rakt på varandra och ökar längre bort från mittpunkten. Den kompensation som görs är att de tider som den radioaktiva pelleten stannar på de förbestämda positionerna ändras. Ju längre bort från mittpunkten desto större minskning eller ökning av tiden som pelleten står stilla i just den stoppositionen.

Värdena som användes vid försöken kom från dosfördelningsmatriserna från den självframkallande filmen och var de som var positionerade rakt genom tråden. Det gav en bättre överensstämmelse nära källorna medan det gav en sämre längre ifrån. Resultaten av kompensationen visar att det är möjligt att återskapa dosfördelningen hos tråden genom att ändra tiderna för de olika stoppositionerna.

Arbetet utfört av **Daniel Gasic**
Handledare: Jens M. Edmund
Examensarbete på 30 hp
Avdelningen för medicinsk strålningsfysik, Lunds universitet
Arbetet utfördes på universitetssjukhuset i Herlev, Danmark

Brachytherapy of Squamous Cell Carcinoma in the Lip: MDR to PDR Treatment Conversion

Introduction: From 1988 – 2004, patients with squamous cell carcinoma in the lower lip were treated with medium dose rate (MDR) ^{192}Ir wires using a manual afterloading technique. An average of 3 wires were used, each with a mean length of 36 mm (range 27 – 65 mm) and a mean dose rate of 4.5 Gy/h (range 1.8 – 8.7 Gy/h). The average prescribed dose was 21.5 Gy (range 21.0 – 32.6 Gy) at the 85% isodose of the basal dose point according to the Paris system. The main purpose of this study is to investigate the equivalence of dose distribution when replacing a manually afterloaded wire with a remotely controlled stepping source. This treatment conversion is considered primarily because of improvements in staff radiation protection and hospital logistics.

Materials and methods: The ^{192}Ir wire dose distribution plans were previously calculated in Nucletron Planning system, module MPS v11.33® (NPS). These plans were compared to plans with a reconstructed wire (RW) that is planned and calculated in PLATO, module BPS v14.2.3® (PLATO). The RW is a catheter of 36 mm that contains a ^{192}Ir stepping source with equally weighted dwell times separated by either 2.5, 5, 7.5 or 10 mm step length. The comparison of dose distribution difference between the RW plans and the actual wire measurements, made with GAFCHROMIC® EBT2 film, was performed using an in house program developed in MATLAB®.

Results: For the midplane parallel to the wire, the prescribed isodose differs just above 2% at equal distances and the distance less than 0.14 mm at equal isodoses for angles smaller than 50º. For the midplane perpendicular to the wire, the difference between the two TPS is just above 1% and less than 0.07 mm for all angles. These results are for RW-4, which is the RW that shows worst agreement in the dose calculation difference. The RW and wire dose distribution is in better agreement at planes further away from the sources. The difference at 1 mm from the midplane is approximately ±20%, about the same difference at 6 mm and less than ±15% at 11 mm evaluation distance. The same trend can be seen no matter what RW is being used. There is an obvious difference the closer the point of interest is to the source. Further away from the source the dose distribution gets smeared out making it difficult to get any conclusive results. Results from the ratio between dose values show a better compliance close to the source, which indicates a large angular dependence. A correction of the dwell weights results in better agreement close to the source.

Conclusion: The difference between NPS and PLATO are mainly because of the difference between AL and EL but also due to the approximations made by NPS, which are insufficient in capturing the change in source specific attenuation properties. There is a general under dosage outside the catheter and cold spots between source positions for longer step lengths but also hot spots at the actual dwell positions. The differences in dose distribution are mainly due to that the AL is not the same as the EL. Another reason is that equal dwell weights were used initially. The different distance of the point of interest will also have impact on the results; a better agreement closer to the source. A better agreement in dose distribution can be obtained by manipulating the dwell weights.

Composed by **Daniel Gasic**
Advisor: Jens M. Edmund
Degree project of 30 credits
Department of Radiation Physics, Lund University, Sweden
The work was carried out at the department of oncology, Copenhagen University Hospital, Herlev, Denmark

Abbreviations and Symbols

.DAT – DATA file (Contains data in ASCII-format, which is delimited by a space)

.TIFF – Tagged Image File Format

.TXT – Text file (in this case ASCII – text file/UTF-8 – text file

AAPM – American Association of Physicists in Medicine

AISI – American Iron and Steel Institute

AL – Active Length

ALARA – As Low As Reasonable Achievable

ASCII – American Standard Code for Information Interchange (a type of character-encoding scheme based on the ordering of the English alphabet)

BD – Basal Dose rate

CLDR – Continuous Low Dose Rate

CT – Computed Tomography

EL – Equivalent active Length

HDR – High Dose Rate

ICRU – International Commission on Radiation Units and measurements

ICWG – Interstitial Collaborative Working Group

ISP – International Specialty Products Inc.

LDR – Low Dose Rate

MDR – Medium Dose Rate

NPS – Nucletron Planning System, with module MPS v11.33®

OMP – Oncentra MasterPlan v3.2®

PDR – Pulsed Dose Rate

PLATO – PLATO patient selection system, PLATO PSS v3.3.2 with brachytherapy module PLATO BPS v14.2.3®

PTW – Physikalisch Technische Werkstätten

QD+ – Quality Dosimetry Plus

RW – Reconstructed Wire

SCC – Squamous Cell Carcinoma

TG-43 – Task Group 43

TPS – Treatment Planning System

$(\Gamma_\delta)_x$ – Exposure rate constant

$\bar{\phi}_{an}$ – Anisotropy constant

θ – The angle between the point of interest and the transverse plane of the source

Λ – Dose rate constant

δ – The energy cut off

α and β – Isotope specific constants

Θ – The angle between both ends of the source

$(\mu_{en}/\rho)_{\text{air}}^{\text{tissue}}$ – The mean mass energy absorption coefficient in tissue and air

Absorbed dose is denoted as dose throughout this report since neither equivalent dose nor effective dose is used.

Table of Contents

INTRODUCTION **1**

BACKGROUND 2
PURPOSE 2

THEORY **3**

THE PARIS SYSTEM 7
REMOTE AFTERLOADING TECHNOLOGY 9
PULSED DOSE RATE BRACHYTHERAPY 10
IRIDIUM-192 11
GAFCHROMIC® EBT2 DOSIMETRY FILM 13

MATERIALS AND METHODS **15**

DOSE CALCULATION DIFFERENCE 15
WIRE MEASUREMENTS 17
CALIBRATING THE FILM 20
STEPPING SOURCE 21
CREATION OF TREATMENT PLANS 22
MATLAB® COMPARISON 23
CORRECTION OF DWELL WEIGHTS 24

RESULTS AND DISCUSSION **25**

FILM CALIBRATION 25
DOSE CALCULATION DIFFERENCE 25
TREATMENT PLANS COMPARED WITH WIRE MEASUREMENTS 28
1 mm Distance *28*
6 mm Distance *33*
11 mm Distance *37*
DOSE DIFFERENCE AND VARIATION 41
CORRECTION OF DWELL WEIGHTS 41
1 mm Distance *42*
6 mm Distance *43*
11 mm Distance *45*

CONCLUSIONS **47**

ACKNOWLEDGEMENTS **48**

BIBLIOGRAPHY **49**

Introduction

Brachytherapy offers the possibility to deliver high absorbed dose to the tumor, with minimal absorbed dose to the surrounding normal tissue. This combination results in an increase of the therapeutic ratio, which allows for a better tumor control with minimal toxicity [1]. The use of brachytherapy allows for tumor control without the need for resection, which is especially important in head and neck cancers where it can cause significant functional and cosmetic destruction [2]. However, surgery is often considered the modality of choice for early squamous cell carcinoma of the lower lip while more advanced stages are treated with brachytherapy though it is possible to treat many early tumors with brachytherapy alone [2]. The first aim of treatment in lip cancer is nevertheless, a good local control, secondary is a good cosmetic and functional result.

In brachytherapy, various treatment planning systems (TPS) are available for usage. The difference between them lies not only in the hardware but also in the underlying physics of the dose calculations. There are many impacts for the user because of these differences, which include accuracy of source reconstruction, calculated dose, speed of dose calculation as well as other factors. It is of great importance to understand the algorithms and approximations used for dose calculations so that a comparison of dose to the patient between different TPS and film measurements can be investigated and if necessary corrected for.

Cancer in the lip is one of the most common malignant tumors and accounts for 30-45% of oral cavity cancers, 90-96% of these are squamous cell carcinomas (SCC) and are usually located in the lower lip [3-6]. Well differentiated lip cancer occurs predominantly (around 90%) in males and most of the tumors are discovered after the patients have reached the age of 60 years [5, 7-8]. However, this type of tumor is often detected in an early stage since the majority of all SCC are located on the vermillion border of the lower lip [9]. This means that the treatment often is of small tumors without lymph node involvement, and engenders a promising prognosis [10].

Patients with recurrent cancers have often already been treated with surgery and or external beam irradiation. Therefore it can be very difficult to treat the recurrence without dealing to much tissue damage to the patient. It is often only possible to re-irradiate these patients with brachytherapy because of the minimal absorbed dose to the surrounding healthy tissue [2].

Background

At Herlev University hospital in Denmark, patients with squamous cell carcinoma in the lower lip has previously (1988-2004) been treated with a manual afterloading technique at medium dose rate (MDR, yielding around 5 Gy/h) using ^{192}Ir wires. The treatment consisted of one fraction in which the wires were placed with a maximum distance of 10 mm apart for 4 to 5 hours resulting in an average absorbed dose of 21,5 Gy (range 21.0 – 32.6 Gy) prescribed at the 85% isodose of the basal dose point according to the Paris system. An average of 3 wires were used, each with a mean length of 36 mm (range 27 – 65 mm) and a mean dose rate of 4.5 Gy/h (range 1.8 – 8.7 Gy/h). Between 1988 and 2004, 87 patients were treated with this technique. The local failure was 7% and complications were observed in some cases. There were functional complications in 3.4% of the cases while there were cosmetic complications in 5.7% of the cases.

Recently, a new computerized remote ^{192}Ir afterloading system has been installed at Herlev hospital, offering the possibility of providing both high dose rate (HDR) treatments and pulsed dose rate (PDR) treatments. The treatment conversion from MDR wire treatment to PDR treatment with a remote afterloader is considered primarily because of problems associated with the radiation protection and hospital logistics. It would therefore be advantageous to carry out the lip treatment with a stepping source remote afterloader using a pulsed dose rate treatment schedule.

Purpose

The main purpose of this project is to establish whether it is possible to reproduce the MDR wire treatment with a PDR stepping source treatment within the same treatment time of 4 to 5 hours. The different aspects of the dose traceability at the prescribed isodose, when converting the treatment from a continuous MDR to a PDR that results in an equivalent tumor control, needs to be investigated. Dose algorithms and reported doses in the MDR and PDR systems will be compared and relevant corrections are to be quantified. One step is to investigate the change in dose distribution of one ^{192}Ir wire of average length when the wire is reconstructed by an ^{192}Ir remotely afterloaded stepping source.

Theory

Treatment planning for patients treated with ^{192}Ir wire was previously done using Nucletron planning system[i]® (NPS). This software uses a classical formalism to calculate the dose rate of the wire and subsequently the absorbed dose to water [11]. The more recent developed TPS, such as PLATO patient selection system[ii]® (PLATO) and Oncentra MasterPlan[iii]® (OMP), use a worldwide accepted formalism recommended by the American Association of Physicists in Medicine (AAPM), Task Group 43 (TG-43) for dose calculations [12-13]. The recommended protocols for dose calculation formalism are based on measurable quantities and data derived from Monte Carlo calculations. The dosimetry data endorsed by AAPM Report No. 43 results in moderately large absolute dose rate changes relative to traditionally used treatment planning data [14-16].

The dose calculation formalism that is used by obsolete TPS, such as the one previously used at Herlev hospital, uses classical methods such as exposure rate constants and tissue attenuation factors in contrast to the new formalism of TG-43 that uses dose rates from actual sources in a tissue equivalent material. A classical method to calculate dose rate in water, $\dot{D}(r)$, at a specific distance, *r*, is calculated using the point source approximation

$$\dot{D}(r) = A_{app} \cdot f_{med} \cdot (\Gamma_\delta)_x \cdot \frac{1}{r^2} \cdot T(r) \cdot \bar{\phi}_{an} \qquad (1)$$

where A_{app} is the apparent activity of the source, the f_{med} is the exposure to dose conversion factor from air to water and the $(\Gamma_\delta)_x$ is the exposure rate constant in air of the radionuclide. $T(r)$ and $\bar{\phi}_{an}$ is the tissue attenuation factor and the anisotropy constant, respectively. One of the primary issues with this formalism is that it is based on photon fluence around an ideal source while clinical applications require dose distributions within the patient since it takes the scattering and attenuation in tissue and encapsulation into account.

Interstitial Collaborative Working Group (ICWG) describes a formalism regarding high intensity sources (used for HDR and PDR) for interstitial brachytherapy. This formalism is endorsed and recommended by AAPM TG-43. The dose calculation algorithm is constructed so that the dose can be calculated at any point, (r, θ), relative to the source centre where *r* is the distance to the point of interest and θ is the angle between the point of interest, $P(r, \theta)$, and the transverse axis of the source. The transverse plane bisects the active source

[i] with module MPS v11.33
[ii] PLATO PSS v3.3.2 with brachytherapy module PLATO BPS v14.2.3
[iii] v3.2

by definition and specifies the origin of the dose calculation formalism. The point of interest, where the dose is evaluated, is specified by polar coordinates (figure 1). The dose rate in water at the point of interest, $\dot{D}(r,\theta)$, is given by

$$\dot{D}(r,\theta) = S_K \cdot \Lambda \cdot \frac{G_x(r,\theta)}{G_x(r_0,\theta_0)} \cdot g_x(r) \cdot F(r,\theta) \quad (2)$$

S_K is the air kerma strength and Λ is the dose rate constant. A geometry function is described by $G_x(r,\theta)$, while $g_x(r)$ and $F(r,\theta)$ are the radial dose and anisotropy function, respectively. The subscript "x" is explained and denoted differently in the sections of geometry factor and radial dose function respectively (Eq. 5 and Eq. 6). All quantities that the formalism applies are defined in terms of a sparsely distributed grid of dose rates derived from either Monte Carlo calculations or dosimetry measurements [17]. Apparent activity multiplied with the exposure rate constant has been replaced by air kerma strength, the exposure to dose conversion factor with the dose rate constant, inverse square law with geometry factor, tissue attenuation factor with radial dose function and the anisotropy constant was replaced by the anisotropy function (Eq. 1 and 2).

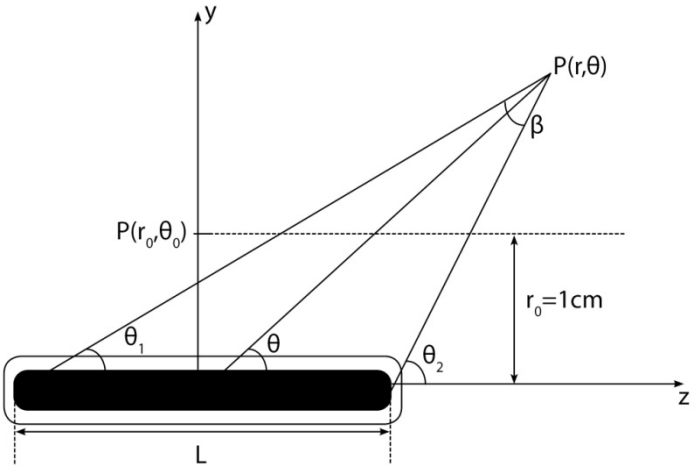

Figure 1: *Illustration of the geometry assumed in the dose calculation formalism.*

Air kerma strength is a measure of source strength, which is specified in terms of air kerma rate at a point, in free space, $K(d)$, along the source transverse axis. Eq. 3 shows how air kerma strength and air kerma rate is related.

$$S_K = \dot{K}_\delta(d) \cdot d^2 \quad (3)$$

Air kerma strength is numerically identical to the reference air kerma rate, which is recommended by ICRU 38 and 60 [18-20]. Air kerma strength is equivalent to the air kerma rate, $\dot{K}_{\delta}(d)$, corrected for photon attenuation, for photons with energy greater than δ, and scattering in any medium between the source and detector. The energy cutoff, δ, is intended to exclude low energy and contaminant photons, which increase the air kerma rate without contributing to absorbed dose at distances greater than 0.1 cm in tissue or equivalent medium. The value of the energy cutoff is typically 5 keV for brachytherapy sources [21].

The definition of the dose rate constant is the dose rate to water at a distance of 1 cm on the transverse axis of a unit of air kerma strength in a water phantom (Eq. 4).

$$\Lambda = \frac{D(r_0,\theta_0)}{S_K} \tag{4}$$

The dose rate constant includes the effect of source geometry and encapsulation as well as self-filtration and spatial distribution of the activity within the source. The constant also include scattering in the surrounding water, which is the reference medium for describing dose rate around brachytherapy sources.

The geometry factor ignores the scattering and absorption within the source itself and only accounts for the variation of the relative dose due to spatial distribution of activity (Eq. 5).

$$\begin{aligned} G_P(r,\theta) &= r^{-2} \\ G_L(r,\theta) &= \begin{cases} \frac{\beta}{L \cdot r \cdot \sin\theta} & \theta \neq 0° \\ (r^2 - L^2/4)^{-1} & \theta = 0° \end{cases} \end{aligned} \tag{5}$$

The subscript "P" and "L" has been added in AAPM TG-43 update and denotes whether a point source or line source approximation, respectively, is used [12]. The angle,β, in radians, is the angle between both ends of the source with respect to the point of interest while the term L denotes the active length of the source.

It is possible to describe the dose falloff by the geometry factor to increase the accuracy of the interpolation near the source since the inverse square law engenders rather large dose gradients [17].

The radial dose function defines the dose rate falloff along the transverse axis of the source due to absorption and scatter in the surrounding medium. The radial dose function is equal to unity at distance 1 cm and is defined by Eq. 6 as explained above. The subscript "x" indicates whether a point source "*P*", or line source "*L*", geometry function was used in transforming the data to the new dose calculation formalism.

$$g_x(r) = \frac{\dot{D}(r,\theta_0)}{\dot{D}(r_0,\theta_0)} \cdot \frac{G_x(r_0,\theta_0)}{G_x(r,\theta_0)} \tag{6}$$

The anisotropy of the dose distribution around the source, including effects of absorption and scatter in the surrounding medium as well as encapsulation, is described by the anisotropy function and is defined by Eq. 7, which shows the two-dimensional anisotropy function.

$$F(r,\theta) = \frac{\dot{D}(r,\theta)}{\dot{D}(r,\theta_0)} \cdot \frac{G_L(r,\theta_0)}{G_L(r,\theta)} \tag{7}$$

There are both one-dimensional and two-dimensional methods to calculate the anisotropy function. The two-dimensional approach is utilized to calculate the anisotropy function for a cylindrically symmetric line source (figure 1) while the anisotropy function for a point source is calculated using the one-dimensional method.

As explained earlier in this section, depending on when the TPS was developed and released, it utilizes either a classical formalism or TG-43 more recent formalism when calculating the dose in water. The dose algorithms based on a traditional formalism uses isotope specific approximations such as the Meisberger approximation and uniform anisotropy. The Meisberger approximation is an approximation of the exposure in water divided by exposure in air with a third order polynomial [22-26]. The more recent formalism, based on AAPM TG-43, uses source specific data instead.

The calculations in NPS are based on Eq. 1 for a line source, e.g. a wire. The dose rate in water, $\dot{D}(r,\theta)$, at the point of interest is given by Eq. 8 [27],

$$\dot{D}(r,\theta) = f_{med} \cdot \Gamma_\delta \cdot A_{app} \cdot \frac{\Theta_r}{d} \cdot S(d) \tag{8}$$

where Θ_r is the angle between both ends of the source, seen from the point of interest and d is the perpendicular distance from the point of interest to the source axis. $S(d)$ is given by

$$S(d) = \frac{1+\alpha \cdot d^2}{1+\beta \cdot d^2} \quad (9)$$

The function $S(d)$ describes the absorption and scattering along a distance d in tissue or equivalent medium [28]. The constants α and β are isotope specific. The values α = 0.00010 cm^{-2} and β = 0.00050 cm^{-2} are used by NPS for ^{192}Ir, which is the radionuclide used in this study [29]. The difference between the expression in Eq. 9, called the Van Kleffens and Star expression, and the more commonly used Meisberger relationship is less than 1% for distances less than 9 cm [22, 28, 30-32]. For greater distances, it is better to use the Van Kleffens and Star expression since it gives more realistic values of the absorption and scatter factor for ^{192}Ir sources [22, 28, 30]. Table 11 in the appendix section shows a more detailed explanation of the Meisberger approximation and the Van Kleffens and Star expression.

It is possible to see the connection between Eq. 1 and 8 and how they are related since Eq. 8 has only been modified from the classical formalism, to utilize the van Kleffens and Star expression.

The Paris System

The Paris system is a well known and worldwide used dosimetry system. The Paris system is one of several dosage systems whose function is to set a foundation of which the TPS can plan a treatment that will deliver the highest possible minimum dose to the selected target volume. The highest doses will occur around the active sources and these must be small enough to avoid undue necrosis but also large enough so that the prescribed dose will cover the target volume. Different dosimetry systems distinguish themselves in several ways and differ in, among other ways, the rules of implantation e.g. the sources arrangement throughout the target volume, in the definition in dose uniformity and in the method recommended for prescribing the dose i.e. for the calculation of the reference dose rate [33].

All interstitial treatment techniques e.g. ^{192}Ir wires and stepping sources, which are implanted within tissue creates areas of very high dose in the immediate vicinity if the sources. The dose reduces rapidly with increased distance. The Paris system adjusts the source spacing and source length within limits to match the target volume dimensions [34].

The basal doses, which are points of low dose gradient located inside the target volume defined by a number of sources, are used by the Paris system together with target volume dimensions to create functions of geometrical relationships between the sources.

According to Pierquin et al. 1987, [35], the Paris system is based upon three principles:

- The radioactive sources must be rectilinear and parallel. They also must be arranged so that their centers are positioned in the same plane. This plane is called the central plane and must be perpendicular to the direction of the sources.
- The reference linear air kerma strength must be uniform and identical for all sources.
- Adjacent sources must be placed so that there is equidistance between them.

The principle of equal spacing between lines and the shape of the target volume leads to, for multiplanar implants, implantation in squares or triangles [36]. This is also shown in figure 43 in the appendix section. There are usually no problems with inhomogenous dose distribution since the Paris system requires that all linear sources with activity along the whole length of each line be constant and identical.

The dose is calculated and prescribed to the reference isodose, which is 85% of the basal dose rate (BD). The BD is the arithmetic mean of the local minimum dose rates (figure 43). The dose is specified in the central plane of the application and is referred to as the BD or the basal dose point. The reference isodose is a fixed percentage of the BD so that the reference dose is located outside the volume defined by the sources. The reference isodose surface should encompass the whole target volume if the recommendations of the Paris system are followed. The BD depends on the geometry of the implant, the linear air kerma rate of the source and on the radionuclide used.

The minimum dose rate points in the central plane occur for single plane implants in the middle between adjacent lines as is shown in figure 43a. These points occur for multiplanar implants at the geometric centers of triangles or squares, which are formed by the sources in the central plane (figure 43b and 43c).

The high dose region (also known as the hyper dose sleeve) is defined by the Paris system as the volume of tissue immediately surrounding the source and receives a dose equal to or greater than twice the reference dose. The risk of exceeding normal-tissue tolerance, which can lead to treatment complications, e.g. necrosis, occur when this regions diameter exceeds 8 – 10 mm [35-37]. This is a constraint that will limit the spacing of the sources. There is, however,

in principle substantial freedom in choosing the arrangement and spacing between sources when using the Paris system.

Remote Afterloading Technology

The earliest remote afterloading devices were developed in the early 1960's and used for brachytherapy in England and the United States.

Afterloading is a technique where the applicator is first placed into the target position and the radioactive sources are loaded into the applicator afterwards. Afterloading can either be made by hand (manual afterloading), mechanically with hand-driven devices (mechanical afterloading) or by computerized machines (remote afterloading). When the applicator contains the radioactive sources at the time of placement into the patient, it is called hot loading. Hot loading and manually afterloading was used prior to the development of remote afterloading technology.

Radiation doses can be delivered using

- Low dose rate (LDR) <2 Gy/h
- Medium dose rate (MDR) 2-12 Gy/h
- High dose rate (HDR) >12 Gy/h

and the treatment time obviously depends on the dose rate [19].

As low as reasonable achievable (ALARA) is a well established and acknowledged principle in radiation control and replacing the older technologies (hot loading and manual afterloading) with automatic remote afterloading, can reduce radiation exposure to medical personnel (oncologists, physicists, attending physicians, nurses and other health personnel).

Remote afterloading provides technical advantages such as reducing the venture of misplacing or losing the sources. With the software it also offers isodose distribution optimization that improves dose conformity.

Patients treated with MDR brachytherapy can receive more nursing care while the source is retracted and kept within the vault in the machine between the pulses. Both the patients and their relatives often appreciate this since the patients can be visited during the treatment.

High dose rate and medium dose rate remote afterloading treatments are probably preferable at facilities with large patient populations since if they were treated with conventional LDR brachytherapy the treatment would require prolonged hospitalizations. There is, however, treatments were low dose rate is required to obtain the best possible tumor control. Longer therapy sessions

contribute to prolonged hospital stays were one problem is undesired applicator movement. Applicators can be rigidly secured for at short period of time.

Remote afterloading technology is not free of disadvantages. The devices are costly and often require a renovation of conventional hospital rooms.

Patient misadministration as well as radiation emergencies can still occur due to errors caused by the operator by entering incorrect treatment parameters. The source guide tubes can get detached from both the machine and patient and the source itself can become lodged in the guide tubes.

The advantages of remote afterloading devices appears however to outweigh the disadvantages which means that several clinics transitions to this technology.

Pulsed Dose Rate Brachytherapy

Pulsed dose rate brachytherapy is a technique introduced in the early 1990's, intended to replace continuous low dose rate (CLDR) brachytherapy given with wires or seeds [38]. Pulsed dose rate generally simulates continuous LDR brachytherapy by administering a highly fractionated treatment. The typical areas where CLDR is given are head and neck cancers, vaginal tumors, tumors of the vulva, cervix and female urethra and prostate cancer. The treatment is applied as primary therapy, boost, palliation or salvage for recurrent and highly pre-treated cancers and isolated lymph nodes [39].

With a single small stepping source and a remote afterloading apparatus, the physical dose distribution in terms of conformity and homogeneity, can easily be optimized compared with the commonly applied techniques with linear sources [40-43]. It is a fairly effortless accomplishment to optimize the dose distribution by modulating the dwell times of the stepping source. The possibility of biologic dose optimization is also offered with PDR by addressing time-dose patterns characterized by the dose per pulse, total number of pulses and interpulse periods while keeping the overall treatment time comparable to that for commonly applied CLDR treatments [44-45].

Available emergency procedures are a necessity during treatments in situations of a malfunctioning afterloader unit where the source cannot reach the programmed position or is lodged within the patient [46-47]. There is one major difference between HDR and PDR regarding safety aspects. For HDR, personnel are always in the direct vicinity during administration, which seldom takes longer than 30 minutes. This means that safety measures can be started quickly in case of an accident. In PDR, however, the treatment time can be from several hours up to several days. During this time physics personnel, technicians and engineers will not closely monitor the patient. Therefore it is crucial that nursing personnel are well trained in emergency procedures.

The PDR afterloader devices usually contain a single 1 Ci ^{192}Ir source that is welded on to the end of a transfer cable. Apart from the active source, the machine also contains an identical wire, equipped with a dummy check source. Both wires are stored in the afterloader around a rotatable drum. The PDR treatment consists of a sequence of short pulses generally given at hourly intervals. The average dose rate per hour should correspond to a CLDR treatment and the overall treatment times should be the same. The transition from LDR to PDR is fairly unostentatiously, simply keep the overall dose and the overall time the same and replace the CLDR with a 10-minute pulse every hour to have a treatment equivalent to conventional LDR, both in terms of tumor control and normal tissue effects [44]. A pulse is a fractionation yielding a dose that is less than 1 Gy. Each individual pulse starts with a scan of the complete implant/catheter and transfer tubes with the dummy source. To deliver the dose in a comparable time as with CLDR the activity of the source must be roughly in the same order of magnitude as the total activity of a CLDR treatment. Afterloaders used for PDR operates at somewhat higher activities, around 1 Ci, which allows for sufficient breaks between the pulses. The higher dose rate infers that the treatment must be fractionated to keep the biological effectiveness of LDR. However, this study deals with the possibility to simulate a continuous MDR treatment with a PDR source from a dosimetric point of view.

The repopulation is probably not an issue in brachytherapy, which means that longer treatment times should increase the therapeutic advantage between early and late responding tissues [48]. The biological data for model calculations, their distributions and extreme values are not entirely known. Changes in the fractionation sequences render the choice of values more important. The initial suggestion of equivalence between CLDR at 0.6 Gy/h and a 10-minute pulse of 0.6 Gy every hour is probably reasonable for any combination of biological parameters [48]. Since the proposed PDR regimen differs from the CLDR, the overall treatment time needs to be extended to preserve the therapeutic ratio. The treatment time needs longer extension the more the proposed regimen differs from CLDR [49]. This data can be used as a starting point to investigate the MDR to PDR treatment conversion from a radiobiological point of view.

Iridium-192

Iridium is a hard silvery-white transition metal, which means that the atom has an incomplete "d" sub shell. It has the atomic number 77 and is denoted Ir. When stable ^{191}Ir absorbs a neutron, ^{192}Ir is produced. Nuclear reactors are usually used to neutron activate the iridium. The half-life is 73.827 days and it decays to several excited states of ^{192}Pt (Platinum) through β^- decay, 1.460 MeV, and ^{192}Os (Osmium) through electron capture, 1.046 MeV. The decay scheme for ^{192}Ir is passably complex (figures 41-42 in the appendix section)

and has about 40 different gamma ray emissions with energies ranging from 136 keV to 884 keV, three x-ray emissions of approximately 60 keV, three, less than 10 keV Auger electrons and three β^- electrons with a maximum energy of 672 keV (table 1).

Table 1: *^{192}Ir radiation energies and their occurrences for a few of the decays [iv].*

Type of decay	Energy (keV)	Occurrence (%)
γ	205.79	3.3
γ	295.95	28.7
γ	308.45	29.8
γ	316.50	83.0
γ	468.07	47.8
γ	484.57	3.2
γ	588.58	4.5
γ	604.41	8.1
γ	612.46	5.3
β	256.00 (max)	5.5
β	536.00 (max)	41.3
β	672.00 (max)	48.0

The literature is at variance about the effective energy of the photon emission. Here, the value for the average energy of the emitted photons from an unencapsulated source is 370 keV [50]. Iridium shows a high degree of internal attenuation due to its low effective photon energy and very high density.

For medical treatment, ^{192}Ir can be obtained in the forms of seeds, wires and stepping sources. Seeds are tiny cylindrical sources that are supplied inside strands of nylon of less than 1 mm outside diameter. Seeds deliver low dose rate treatment and are mostly used for permanent implant of prostate cancer treatments. Dosimetry of ^{192}Ir seeds is beyond the scope of this report and is not presented nor discussed further.

A wire is thin and flexible and consists of a radioactive iridium-platinum core that can deliver treatments of LDR to MDR. They have a casing made of pure platinum and are available in different dimensions and activities. Wires are used for interstitial and intracavitary brachytherapy for the treatment of tumors of the head and neck region and breasts [51-53]. They are also used for the treatment of urological, gynecological and anal tumors as well as soft tissue sarcomas and superficially skin tumors [54-56]. Depending on the therapeutic requirements, the wires can be cut up into parts of needed lengths and be used with catheters or needles since the wires are non-sterile.

A stepping source is used in an afterloader system and comes with activities for LDR equivalent, MDR equivalent and HDR treatments. The radioactive

[iv] Data from Eckert & Ziegler BEBIG GmbH, Iridium-192 wires - instructions for use.

source is encapsulated by stainless steel and welded on a steel cable. The active length of the source differs depending on its use. For an example, a PDR source consists of an inactive and an active pellet while a HDR source only has an active core. There are both PDR and HDR sources, however, PDR is more often used to describe a treatment technique. Afterloading systems are replacing the wire treatments and are used for most brachytherapy treatments today since it can be equipped with a source of any activity, often between 1 to 10 Ci.

GAFCHROMIC® EBT2 Dosimetry Film

International Specialty Products Inc. (ISP) develops the film used. The GAFCHROMIC® EBT2 dosimetry film QD+ is self-developing and develops in real-time, i.e. no processing is required. It is formulated to be energy independent from 50 keV into the MeV range and according to the manufacturer, the response to 60 keV photons may be up to 10% greater than the response to 6MV photons. The dose range for the film is 1 cGy – 10 Gy (red color channel) and 1 cGy – 40 Gy (green color channel) and an overall effective atomic number, Z_{eff}, of 6.84 makes it near tissue equivalent (Z_{eff} of water is 7.42). The color of the film is yellow, which arises from the presence of a dye incorporated in the active layer. The principal purpose of this dye, also called a marker dye, is to establish a reference against which the response of the film can be measured.

Since the response of the film is dependent on orientation, all films must be scanned in the same orientation. It is, however, recommended that the films are scanned in landscape orientation since this allows the flatness of the scanner response to be assessed by scanning an unexposed film. It is also important that all exposures are carried out in the same orientation on each piece of film.

The EBT2 film is made by laminating an active film coating to a clear over-laminate film with a pressure sensitive adhesive. The active layer, nominally 30 microns, is coated on a 175 micron, clear polyester substrate, and over-coated with a surface layer or topcoat, nominally 5 microns thick. The over-laminate consists of a 50 micron clear polyester substrate with an acrylate-based, pressure sensitive adhesive of 25 microns nominal thickness (figure 2). The over-laminate protects the active layer/topcoat from mechanical damage. When the film is irradiated by ionizing radiation it changes optical density, which can be detected using a scanner developed for this purpose.

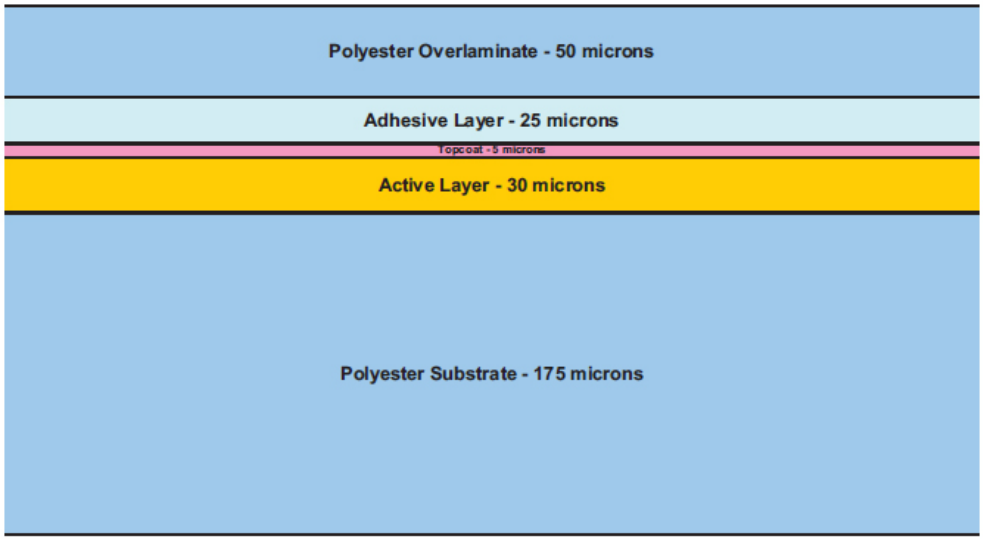

Figure 2: *Configuration of GAFCHROMIC® EBT2 dosimetry film.*

The scanning should be performed using RGB color so that once the scan has been obtained the user can extract the information from the red color channel where the active component in EBT2 film produces its maximum response.

Since the effects of post-exposure changes are proportional to log(time) it is preferable not to scan films immediately after exposure because these errors could have a significant effect on dose accuracy. To keep these errors as small as possible, it is suggested to wait at least 1-2 hours after exposure before scanning the film.

The field flatness of an individual scanner is consistent, and can be characterized and compensated for by obtaining a scan image of an unexposed film. The mean value of this response of this image is measured, and then the responses of each pixel in the image are normalized to the mean value of the response.

Materials and Methods

There were two major parts regarding the dose distribution to be investigated. The first part was to examine how much the two TPS (PLATO using AAPM formalism and NPS utilizing a classical formalism) differed in calculating the dose distribution and the second and most important part dealt with the dose distribution delivered by the wire measured with film and the calculated dose distribution from a stepping source using PLATO.

Dose Calculation Difference

The ^{192}Ir wire dose distribution was calculated in NPS before the treatment of the patient. The plan was calculated so that the prescribed dose covered the volume outlined by the 85% isodose of the basal dose point. The outlining was done automatically in the TPS by specifying the isodose percentage or dose points. The reconstructed wire (RW) is a catheter/needle of arbitrary length that contains an ^{192}Ir stepping source with equally weighted dwell times separated by 2.5, 5 or 10 mm step-length. The step-lengths used are already programmed in PLATO, which means that the dose distribution has to be recreated using these. However, by creating a RW with 2.5 mm step length and weighting the dwell time to 0 for all dwell positions except every third, a step length of 7.5 mm can be applied. The dose distribution of the RW was calculated in PLATO. The length of the RW was chosen to be the same as the length of the wire. However, the active length (AL) between the wire and the RW will always be different because of the small source in the afterloader. The AL of the wire is 36 mm. The equivalent active length (EL) of the RW using 2.5 mm step length is either 35 mm or 37.5 mm and the EL of the RW using 5.0 mm step length is either 35 mm or 40 mm. When using a RW with 7.5 mm or 10 mm step length, the EL is 37.5 mm and 40 mm, respectively (table 2). However, there only exists equivalence between the RW and the wire when Eq. 10 is fulfilled, the separation between sources is denoted as *s* and number of dwell positions is referred to as *n*.

$$AL = EL = n \cdot s \tag{10}$$

Due to the fact that it is not possible to obtain equivalence when reconstructing a wire of average length, 36 mm, the closest possible value around 36 mm for both 2.5 mm and 5.0 mm step lengths will be used. For 7.5 mm and 10 mm step lengths, the closest possible EL longer than 36 mm will be used as EL since the closest possible EL shorter than 36 mm differs too much from the AL.

Note: The closest possible value for a 2.5 mm and 5.0 mm step length is 35 mm. The RW with a length of 36 mm contains either 4, 5, 7, 8, 14 or 15 dwell positions, depending on the step length (table 2). For an uneven number of dwell positions the center of the RW will be in a position of a dwell position, while it, for an even number of dwell positions will be between two dwell positions. Since the dwell position options in PLATO are pre-set, they can not be changed.

Table 2: *Characteristics of the RW and how the different RWs are denoted*

EL (mm)	Number of dwell positions	Step length (mm)	Name of the RW
35	14	2.5	RW-1
37.5	15	2.5	RW-2
35	7	5.0	RW-3
40	8	5.0	RW-4
37.5	5	7.5	RW-5
40	4	10	RW-6

Since there is a difference in dose calculation algorithms between the old TPS holding the patient plans and the new TPSs that will be used for future planning of lip cancer treatments, it is important to find how substantial this variation is. It is most likely OMP that will be the TPS used in the future. There is no difference in the dose calculation algorithm used by PLATO and OMP and a set of points in the programs shows that the largest variation in relative dose is less than 0.12% [57]. The validation was performed by comparing the calculated absolute dose to a group of dose points for each supported source type.

To be able to find the difference between NPS and PLATO/OMP, the dose was checked in a number of points in the two TPS. A basal dose point was positioned 5 mm from the centre of the wire in the midplane in NPS and also 5 mm from the centre of all RWs in the midplane in PLATO. A number of dose points chosen in NPS were inspected on the 85% isodose at different lengths and angles in the parallel and the perpendicular midplane. The definition of the lengths and angles chosen for the parallel midplane is shown in figure 3. All angles chosen lies between the y-axis and the z-axis. This is the upper right quadrant of the coordinate system and it is the same for all other quadrants due to rotational symmetry. The distances are the shortest distance between the centre of the wire/RW and the point of interest, P.

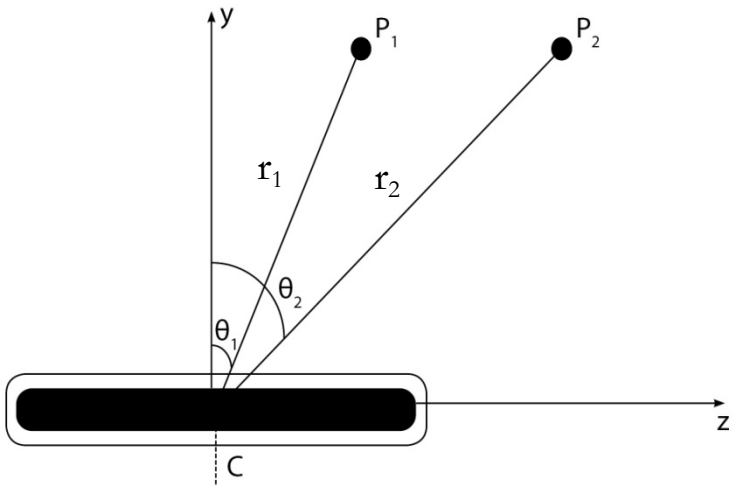

Figure 3: *Shows the angles, θ, and shortest distance, r, to the points, P, from the centre, C, of the source. The points are polar coordinates of the 85% isodose (difference in distance) and equal lengths (difference in dose).*

The coordinates of these points were then introduced around the RW in PLATO and the dose difference between the two TPS at those specific coordinates was calculated. The difference in distance between the 85% isodoses in the two TPS was also calculated at the same angles to investigate differences in treated volume enclosed by the 85% isodose.

Wire Measurements

The wire measurements were performed using GAFCHROMIC® EBT2 dosimetry film QD+ (quality dosimetry plus). To be able to connect the optical density of the film to a dose, e.g. controlling the absolute dose delivered to the film, a calibration curve is needed.

The wires are ordinary ^{192}Ir wires with an outer diameter of 0.3 mm and an active diameter of 0.1 mm, which are amongst the most clinically used wire models but there are of course several different models of ^{192}Ir wires commercially available [58-59]. The wires are very flexible and consist of a radioactive iridium-platinum core and a casing that is made of pure platinum and they are delivered in lengths of either 14 cm or 50 cm. The wire is to be cut to the desired length in clinical practice, so that any length and curvature can be obtained. However, the needles considered here are linear since loops and pins comparisons are out of the scope of this report and rarely used in the treatment of squamous cell carcinoma in the lip. The wires used are manufactured by Eckert & Ziegler, BEBIG GmbH in Berlin and are by them denoted as IRF-1 (Ir2.A81). This source model has previously been studied in the literature using experimental methods and Monte Carlo calculations [60-61].

To deliver a desired dose, e.g. 1 Gy, to the film, the time of exposure was calculated using table 7 and 8 located in the appendix section.

To correctly calculate the film exposure time, the values for air kerma strength and apparent activity supplied by the vendor is used. The calculations are made using both air kerma strength and apparent activity. The apparent activity is multiplied with a gamma factor of 0.109 $\mu Gy/h*MBq^{-1}*m^2$ also supplied by the manufacturer, the gamma factor is compiled by PTB (Physikalisch Technische Bundesanstalt). The values showed in table 7 and 8 are the absorbed dose in cGy/h. They are multiplied with the linear air kerma strength of the wire, which results in the dose rate for a specific length of the wire. With the dose rate/cm wire known, the exposure time can be calculated for any length of the wire needed.

The dosimetry film sheets are 8" x 10" in size and therefore needs cutting before use. The film was cut, using a guillotine cutter, into 2" x 2" for the calibration while the sheets were cut in 4" x 5" for the wire measurements. The films were marked at the edges so that the markings could be zeroed using MATLAB®. If not zeroed, these markings would affect the dose comparison since the scanner detects the markings as well. The film is marked due to the importance of always scanning the film in the same orientation (EBT2 film section).

The wires were placed into a small nylon sleeve using a special apparatus with a built-in ruler. The nylon sleeve was inserted on the left side into the apparatus and the wire on the right side (figures 4-5).

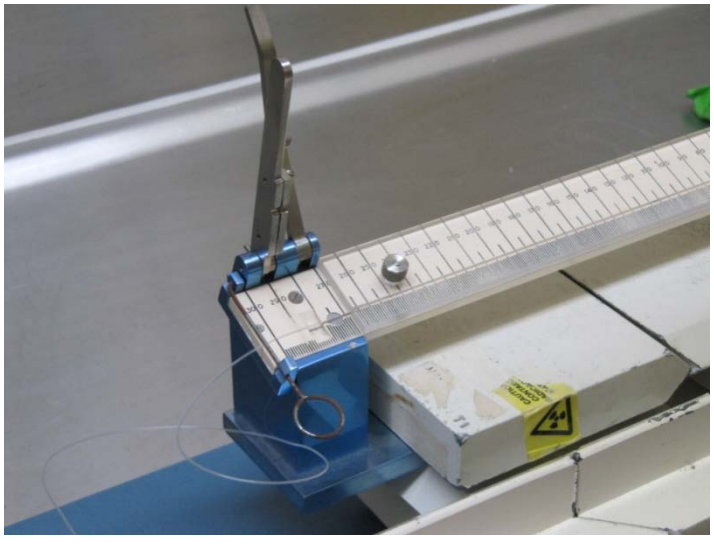

Figure 4: *The apparatus used for placing the wires into the nylon sleeve showing a sleeve inserted.*

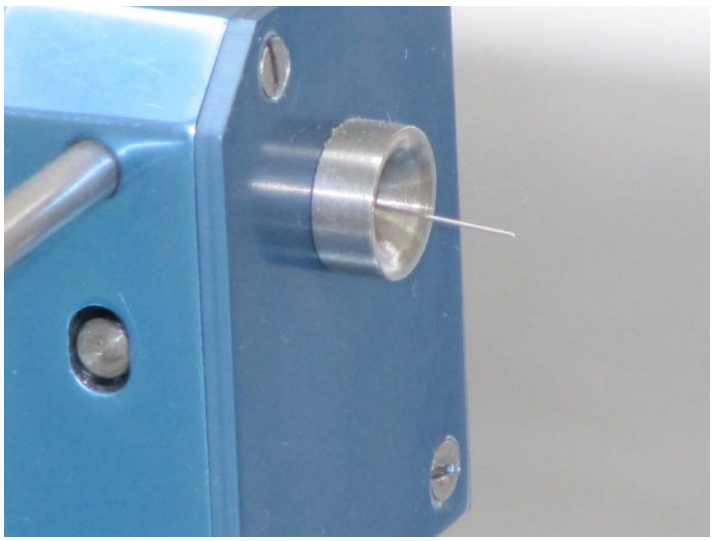

Figure 5: *The far right side of the apparatus used for placing the wires into the nylon sleeve showing a wire inserted.*

The nylon sleeve was then squeezed at both ends to keep the wire in place. This was done so that the wire would be easier to work with, making it longer so that it could be inserted into and pulled out of the needle without any problems with the wire getting stuck within the needle.

The phantom used for the measurements was constructed using polystyrene plates because of their soft tissue resemblance. The films were then placed onto this phantom on the exact same spot for each measurement. To establish backscattering, a 2 cm thick superflab was placed on top of the experimental setup (figure 6). The same geometry was used for each measurement to minimize the uncertainty between measurements.

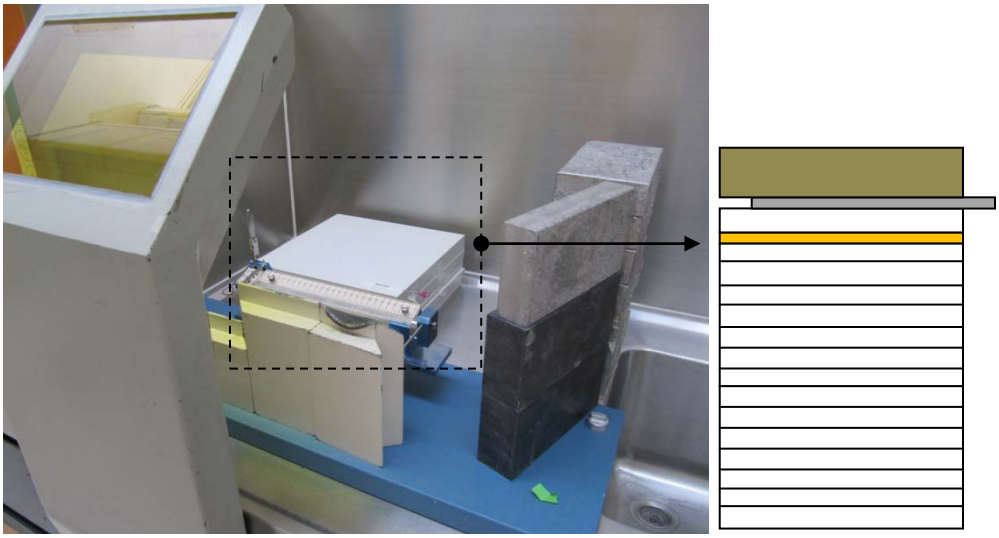

Figure 6: *The experimental setup with the surrounding led shielding. The white sections to the right shows the polystyrene plates, the yellow section show the film and the grey and tan sections shows the needle and superflab, respectively.*

After the measurements, the film was left within a dark envelope for a day before it was scanned. All film measurements got equal "resting time" since the EBT2 films optical density increase over time (EBT2 film section).

The scanner used for scanning the film sheets is of type EPSON Perfection 4990 Photo. The images were scanned using the resolution 50 dpi, saved as .TIFF images and opened via a program called PTW-VeriSoft, which is used to evaluate film measurements. The measured and calibrated dose distribution was exported as a data-file so it could be used for the MATLAB® comparison.

Calibrating the Film

Without calibrating the film, the dose difference can not be obtained using VeriSoft. To be able to check the dose given to the film, the measurement needs to be corrected using the calibration curve. The calibration curve is simply a way of connecting a certain value of the optical density to a specific dose [62]. The optical density is the signal value obtained from scanning the film, which originates from the film response to the irradiation. By using this calibration, VeriSoft can show the absolute dose.

The calibration curve is created using a remote afterloader, of type MicroSelectron® V2 manufactured by Nucletron (Nucletron B.V., Veenendaal, The Netherlands), with a small stepping source of ^{192}Ir with known activity. A number of films are exposed with different doses (0.5, 1.0, 1.5, 2.0, 2.5, 3.0, 3.5, 4.0, 4.5, 5.0, 5.5 and 6.0 Gy) at a distance of 10.85 mm because of the outer diameter of the needle implants. An unexposed film (0 Gy) was also used for the calibration. The film is then scanned and the optical density is coupled with the be-

longing dose. The calibration curve used is shown in figure 8 in the results section.

A calibration curve using 6 MV photons was also obtained using a Varian clinac 2300 iX developed by Varian Medical Systems, Inc., (Palo Alto, CA, USA) to check the energy dependency of the film (figure 44 in the appendix section). As expected, no difference in calibration is observed.

Stepping Source

The stepping source used in this study is a small ^{192}Ir source and a cross section of the source assembly is shown in figure 7. The current source strength during the experiments with the remote afterloader system was 25.42 GBq, which is equal to 0.7 Ci.

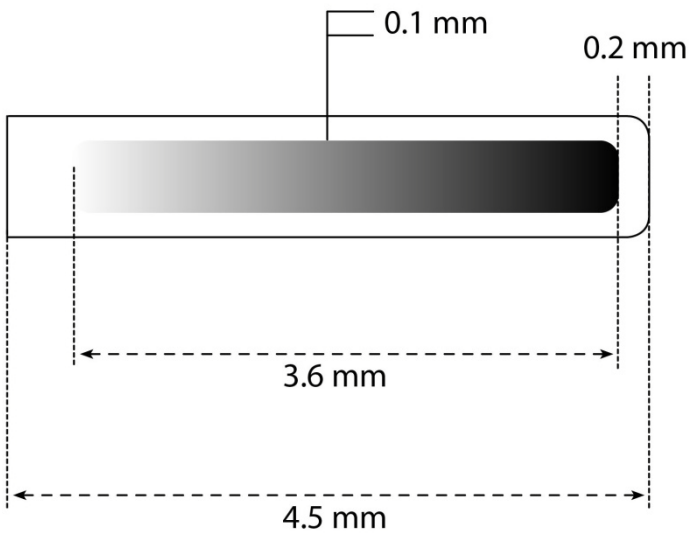

Figure 7: *Cross section of the source assembly, the source is 4.5 mm long and has an active length of 3.6 mm. The steel capsule is 0.1 mm thick at the sides and 0.2 mm thick at the ends. The source outer diameter is 0.9 mm.*

The 0.65 mm diameter source is enclosed in a 0.1 mm / 0.2 mm thick AISI 316L stainless steel capsule, giving the source an outer diameter of 0.9 mm, and has been laser welded to an end of a stainless steel cable [63-64]. The AISI 316L capsule is a very corrosive resistant metal, which is why it is used for this purpose [65]. The source resides in the tungsten safe of the remote afterloader when the system is not in use. The opposite end of the cable is wound around a cable drum. A stepper monitor, which is directly coupled to the cable drum, drives the source cable towards the applicator/needle or retracts it into the safe.

The tail end of the source is color coded and a serial number is engraved in this section as well. The color and engraves have been added so that the source and cable can be identified if needed. This color code is also shown on the monitor connected to the computerized remote afterloader during usage of the equipment. There are different colors for the different sources/cables, active source, dummy source and check cable as well as their movements in and out of the safe.

A beta particle is an electron emitted from the nucleus of a radioactive atom, in this case ^{192}Ir (table 1 and figures 41-42). There exist electron equilibrium for all measurements because of the energies emitted from ^{192}Ir, the thickness of the wire encapsulation and needle implant. To clarify, A 700 keV electron can travel 2.8 mm in water while it is less than 1 mm in stainless steel. The source encapsulation together with the needle implant has a thickness of approximately 1 mm, which means that there will exist electron equilibrium for all measurements. The film does not need electron equilibrium to measure the dose correctly. This fact only points out that all β^- particles are absorbed by the encapsulation making the source a pure γ-emitter.

Creation of Treatment Plans

PLATO was used creating the dose distribution around the RW. The plans were created by first constructing a catheter/needle with its center in origo in the coordinate system and before accepting the construction, the step length of the source must be chosen. Subsequently, the position of the normalization point, also referred to as the basal dose point, was chosen and put at a distance of 5 mm from the catheter in the midplane. This point is put into relation of the catheter, which means that if the catheter is moved, the basal dose point moves with it so that the dose distribution will not change and cause an error. When planning from a CT image it might be more important to keep the basal dose point in relation to an organ or bone structure in which case it is possible to do.

Thereafter a total dose is chosen, also referred to as the prescribed dose to the 85% isodose of the BD, as well as potential marker points and dose points. How the dose distribution is presented to the user is the last action before either exporting the file for MATLAB® to read or to the computerized remote afterloader system for a future treatment.

To be able to export the file, certain requirements must be fulfilled. First, there must be at least three marker points put at different distances away from the reconstructed wire. These marker points must be put in the midplane perpendicular to the RW. If CT-slices are used for the planning this must be done in the IPS-CT module.

The dose distribution must be presented as a three dimensional volume and the resolution (1, 2, 4, 6, 8 or 10 mm) of the presentation and export file must be chosen prior to the export and is defined in the 3D-dose option. The higher the resolution is the larger the generated export file will be since PLATO creates a larger amount of points to present the dose in. The highest possible resolution from PLATO is however only 1 mm, which is the resolution being used in this study. The resolution is perpendicular to the plan parallel to the needle and it will define the resolution in pixels in the images constructed with MATLAB® and the grid margin around the RW. The slice distance of the image series gives the resolution in z-direction in the coordinate system used. However, since only a catheter reconstructed by coordinates is being used the resolution chosen in the 3D-dose option will be the resolution in all directions.

The file generated is called an EVAL-dose file and it is a 3D dose grid file. This file consists of a dose matrix for each plane from the midplane, separated by 1 mm, and it corresponds to the resolution chosen prior to the export.

MATLAB® Comparison

A program was written to evaluate the data obtained during the measurements as well as the data from exported plan files. The program reads the files, .TXT and .DAT depending on if they are exports from PLATO or VeriSoft respectively. Both contain ASCII – formatted data delimited with a space. The program constructs images (shown in the result section of this report) using the data within the files. The data is dose matrices as described in the previous section.

The primarily interest is the percental difference between the PLATO plan, for both 2.5 and 5.0 mm step length, and the wire measurement. The longer step lengths (7.5 and 10 mm) are rejected in an early stage because of its lack in dwell positions within that short RW (36 mm long). To be able to look at the percental difference between the data files, there were some problems that needed to be solved. Since the matrices sizes differ between PLATO and wire measurements, the program needs to create a new coordinate system. Afterwards it aligns both images using the 95% isodoses of D_{max} to locate the sources spatial spread within the image. Because of the newly created coordinate system, the sources locations (within the image) are aligned in such a way that both sources have their centre in the coordinate systems origo.

Furthermore, the program creates a plot over the values located straight through the length of the wire. These plots are used as a first step when trying to correct for the dwell weights.

Correction of Dwell Weights

Since there are some differences between the PLATO plan and wire measurement, a correction is made. The purpose of this correction is to improve the equivalence in dose distribution when matching the RW to the wire. If it is possible to find a correction for these dwell times it will be possible to start the new PDR lip treatment using a computerized remote afterloading system instead of wires. These preliminary results are presented in the end of the results section.

Results and Discussion

This section contains the results, which will be presented and discussed in respective subsection. All results from this study will not be presented due to lack of space and some of the results can refer to the appendix of this report.

Film Calibration

The calibration curve used for the film calibration is shown in figure 8. See figure 44 in the appendix section for the difference between the calibration curves from the small ^{192}Ir stepping source and 6 MV photons from a Varian clinac 2300 iX.

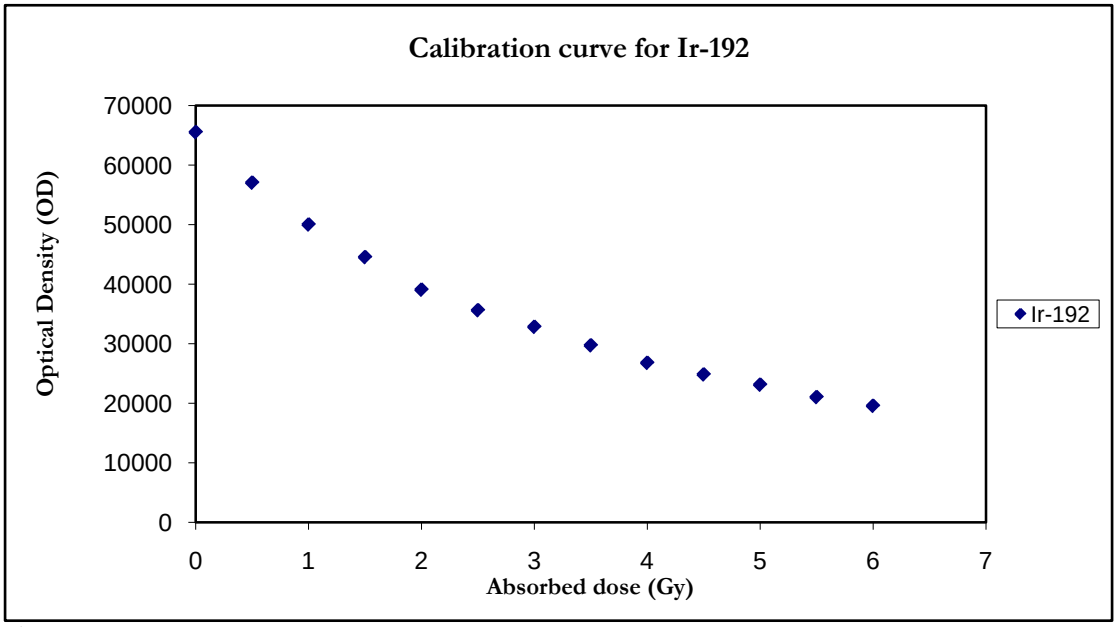

Figure 8: *The curve used for calibrating the EBT2 film.*

Dose Calculation Difference

The results presented next emerge from the investigation of wires of mean length; 36 mm long. For RW-2 in the parallel midplane, the prescribed isodose differs just above 2% at equal lengths for angles smaller than 60º (table 3). For RW-4, it differs just above 2% at equal lengths for angles smaller than 50º (table 3). The difference in dose between the different step lengths at the same angle can be seen in table 3. At equal isodoses for the same angles, the difference in length is 0.18 mm for RW-2 while it is 0.14 mm for RW-4 (table 3).

Table 3: *Presents the results from a 36 mm long wire and needle at two different step lengths for the parallel mid-plane. The results shown are the difference in dose at equal lengths as well as the difference in length at equal isodoses for the eleven points of interest, at different angles from origo in the coordinate system.*

	RW-2		RW-4	
θ	ΔDose (%)	ΔLength (mm)	ΔDose (%)	ΔLength (mm)
0	0.64	0.03	0.93	0.05
10	0.77	0.04	1.13	0.06
20	0.85	0.04	1.37	0.07
30	0.93	0.04	1.55	0.08
40	1.18	0.07	1.72	0.11
45	1.30	0.09	1.89	0.13
50	1.19	0.08	2.06	0.14
60	2.24	0.18	3.77	0.30
70	4.94	0.39	9.41	0.79
80	23.52	0.90	52.27	1.91
90	277.36	0.97	589.61	1.57

Angles from 88.5º to 90º reside inside the needle implants and thus have no clinical relevance. The largest discrepancies of 2% - 239% and 0.18 mm – 0.96 mm for RW-2 can be seen at angles between 60º and 88.5º (table 3). For RW-4, the largest discrepancies of 2% - 509% and 0.14 mm - 1.91 mm can be seen at 50º<θ<88.5º (table 3). These results are also presented in figure 9.

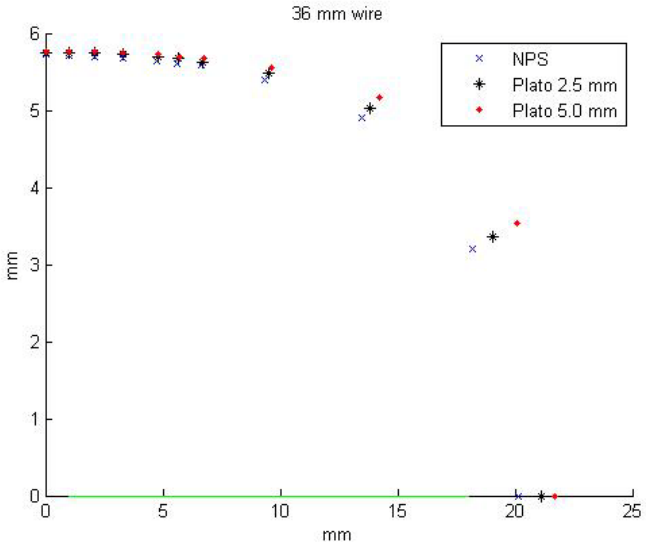

Figure 9: *The difference between NPS and PLATO in the upper right quadrant of the coordinate system in the parallel midplane using a 36 mm long source and needle at two different step lengths (RW-2 and RW-4). The green line represents the wire.*

The first point, at 0º, is the point on the 85% isodose of the basal dose point perpendicular to the centre of the wire in the parallel midplane. The results clearly show that the differences increases further away from 0º.

For the perpendicular midplane, the difference in isodose between the two TPS is less than 1% at equal lengths for RW-2 for all angles (table 4). For RW-4, it differs just above 1% at equal lengths for all angles (table 4). The difference in length at equal isodoses is 0.05 mm or less for RW-2 while it is 0.06 mm or less for RW-4 (table 4).

Table 4: *Presents the results from a 36 mm long wire and needle at two different step lengths for the perpendicular midplane. The results shown are the difference in dose at equal lengths as well as the difference in length at equal isodoses for the eleven points of interest, at different angles from origo in the coordinate system.*

	RW-2		RW-4	
θ	ΔDose (%)	ΔLength (mm)	ΔDose (%)	ΔLength (mm)
0	0.64	0.03	0.93	0.05
10	0.92	0.04	1.21	0.06
20	0.51	0.02	0.81	0.03
30	0.70	0.03	1.00	0.04
40	0.62	0.04	0.92	0.05
45	0.77	0.05	1.07	0.06
50	0.75	0.05	1.05	0.06
60	0.70	0.03	1.00	0.04
70	0.78	0.04	1.07	0.06
80	0.71	0.03	1.00	0.05
90	0.64	0.03	0.93	0.05

The results presented in table 4 are both the difference in length as well as in dose. For the perpendicular midplane there is no trend of larger discrepancies at larger angles and both RWs show a relative small difference in both dose and length for all angles. The results are also presented in figure 10.

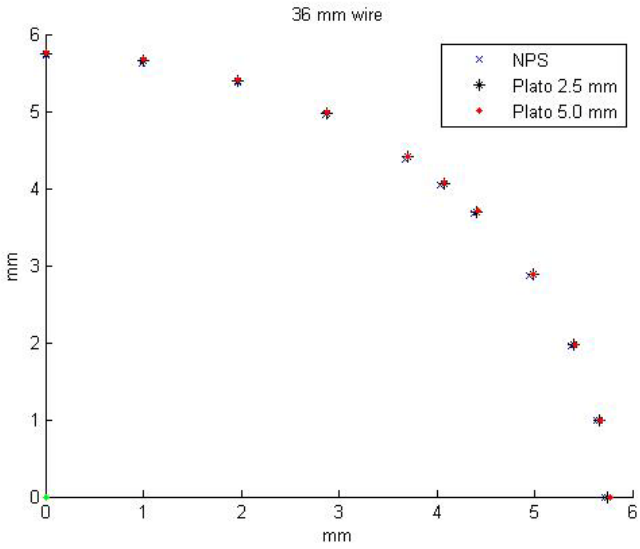

Figure 10: *The difference between NPS and PLATO in the upper right quadrant of the coordinate system in the centre of the perpendicular midplane, using a 36 mm long source and needle at two different step lengths (RW-2 and RW-4). The green dot (0,0) represents the wire.*

It can be seen that for each angle checked there is a greater difference using the 5.0 mm step length. This is due to that the source holds for a longer time in each dwell position, to that equal dwell weights were used as well as due to the different formalisms used by the TPS. It is also, and mostly, due to the difference in equivalent active lengths. This applies to both the parallel and the perpendicular midplane.

The results for RW-1 and RW-3 can be seen in appendix (table 9-10). The results differs mainly that RW-2 and RW-4 show a higher dose from PLATO plans while RW-1 and RW-3 show a higher dose from plans made by NPS. This indicates that the differences are primarily due to the inaccurate equivalent active lengths.

Treatment Plans Compared With Wire Measurements

The comparison using MATLAB® was done specifically at three distances between the centre of the source and film. These distances were 1, 6 and 11 mm. At 1 mm it is easy to see possible hot or cold spots due to the variation in step lengths and active source length. The distance of 6 mm was chosen because this is the region from which the dose often is reported. Since there was no treatment normally given where the wire where supposed to irradiate a tumor that was located more than 10 mm from the wire the distance of 11 mm were chosen to obtain some boundary values.

When calculating the difference, the dose matrices from the PLATO file export were used as first values as is shown in Eq. 11. This means that positive values show a higher dose from PLATO while negative values show a higher dose from the wire measurement. This applies to all figures in this section.

$$D_{difference} = \frac{D_{PLATO} - D_{Wire}}{D_{PLATO}} \tag{11}$$

The reason as to why PLATO was used ahead of OMP is due to the usage of OMP in the clinic.

1 mm Distance

The first three figures (figure 11-13) only show the results before they are compared. Figure 11 is the PLATO file export using 2.5 mm step length, figure 12 is PLATO file export using 5.0 mm step length and figure 13 show the wire measurement. All values are normalized to the highest dose value in each im-

age throughout this section. Figure 11 and 12 clearly shows an evenly distributed dose.

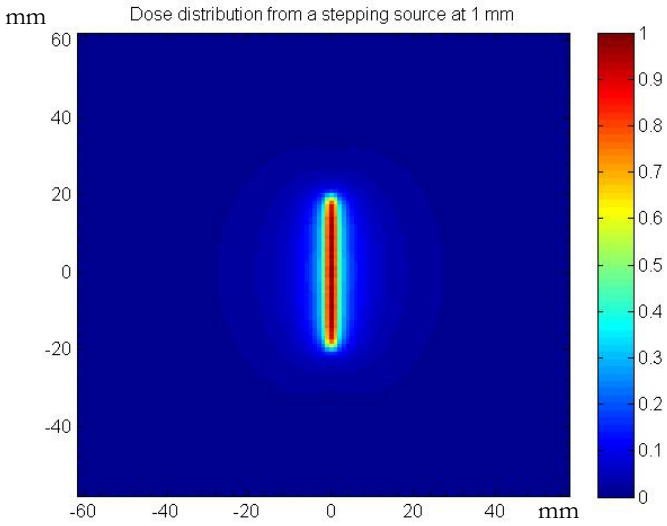

Figure 11: *Dose distribution from the PLATO file export using RW-2.*

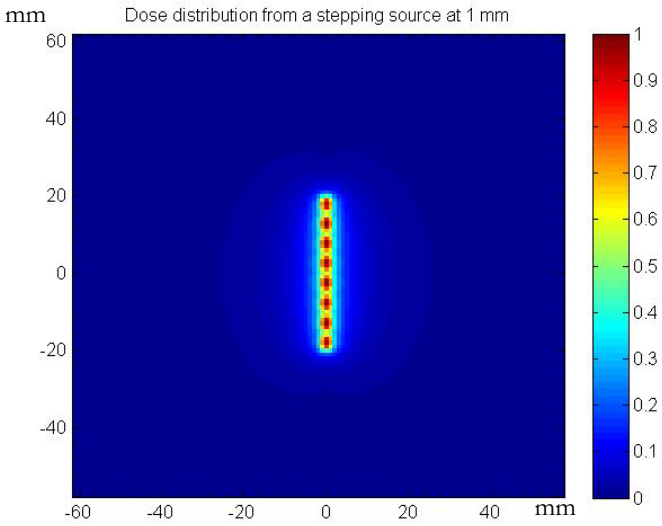

Figure 12: *Dose distribution from the PLATO file export using RW-4.*

Figure 12 clearly show the dwell positions of the source because of the short distance from the source plane. The reason to why the 2.5 mm step lengths did not show in figure 11 is because that there are no cold spots between the dwell positions because of the short distance between them. The dose distributions outside the center of the image show, for the naked eye, some difference in

dose distribution (figure 11 and 12). The 20%-, 40%-, 70%- and 95% isodose levels are the most apparent.

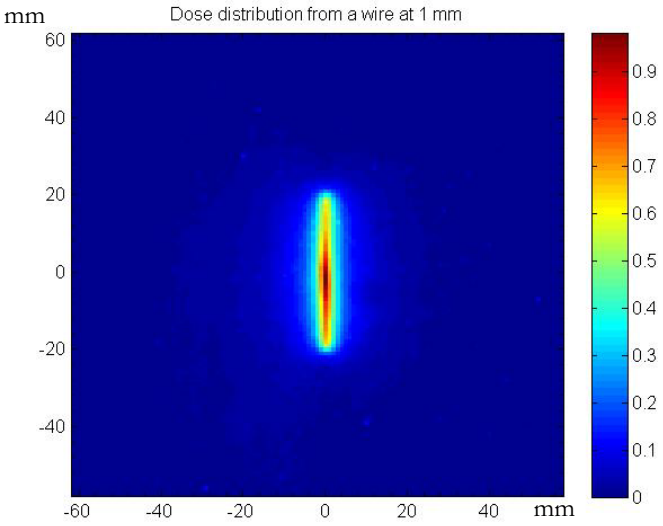

Figure 13: *Dose distribution from the wire measurement.*

Looking closely at figure 13, one can see that the 95% isodose of D_{max} only covers the middle part of the wire. This is however consistent with the general theory that the highest dose rate from a line source is in the center.

Looking at the percental difference (see Eq. 11) between PLATO treatment planning system and wire measurement using EBT2 film, there is an obvious difference (figure 14 and 15).

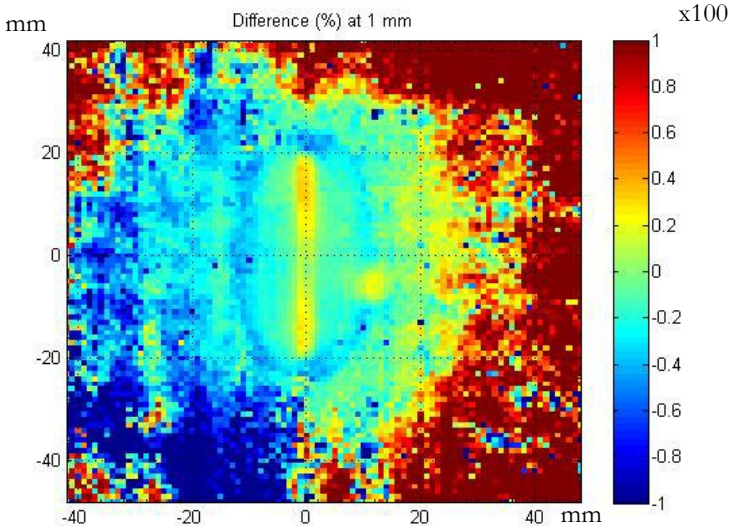

Figure 14: *The percental difference in dose distribution between the PLATO plan and the wire measurement using RW-2.*

Figure 14 shows that there is a bigger difference at the ends of the needle since the 95% isodoses of the PLATO plan and wire measurement differs from each other (figure 11 and 13). The large percental difference in the periphery of the figure is due to the low irradiation in these sectors of the image. This is shown as dark red or blue colors.

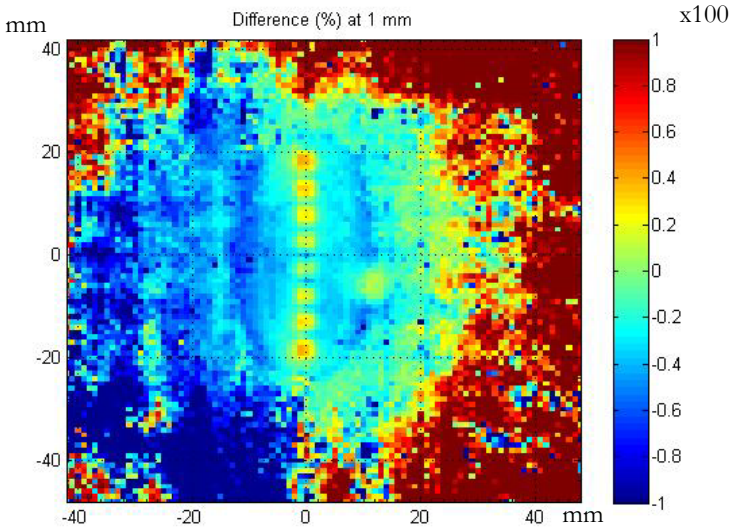

Figure 15: *The percental difference in dose distribution between the PLATO plan and the wire measurement using RW-4.*

It is in figure 15 also possible to see the same trend as in figure 14, bigger difference at the ends of needle. Yet again it is possible to see the dwell positions due to the short distance.

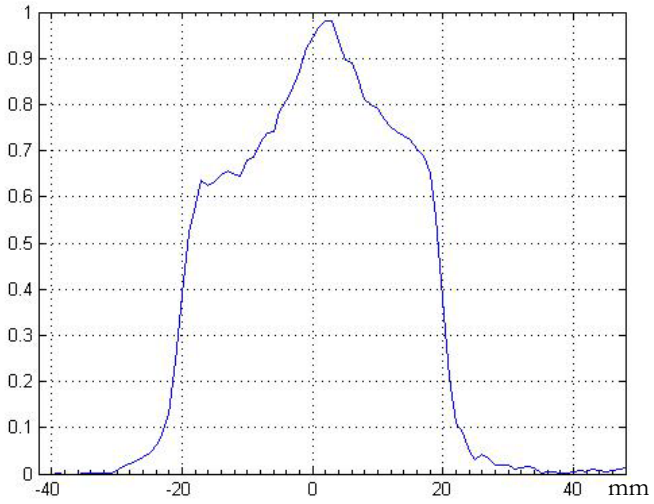

Figure 16: *Shows a plot of the dose distribution from the wire measurement. Plotted values originate straight through the wire at 1 mm distance.*

Plots such as figure 16 were used to correct the dwell weights. The values are the ones in the column of the dose matrix that run through the entire length of the wire.

When using a RW with a smaller EL, the same trend still occur (figure 17). However, using a RW with a shorter EL gives larger cold spots at the ends of the needle. Compare RW-1, which has an EL of 35 mm (figure 17), to RW-2, which has an EL of 37.5 mm (figure 14).

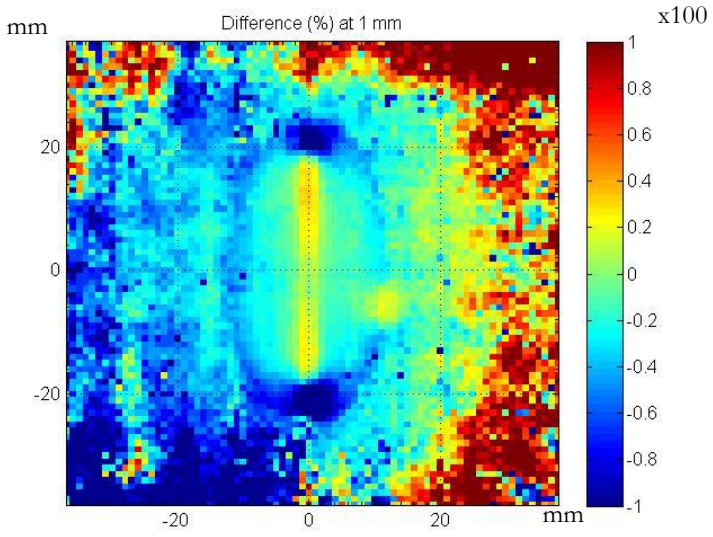

Figure 17: *The percental difference in dose distribution between the PLATO plan and the wire measurement using RW-1.*

6 mm Distance

The first three figures (figure 18-20) only show the results before they are compared using MATLAB®. Figure 18 is the PLATO file export using 2.5 mm step length, figure 19 is PLATO file export using 5.0 mm step length and figure 20 shows the wire measurement. All values are normalized to the highest dose value in each image throughout this section.

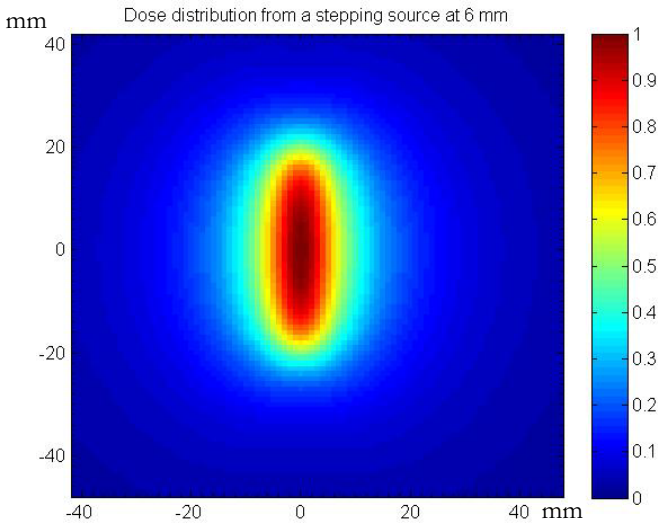

Figure 18: *Dose distribution from PLATO file export using RW-2.*

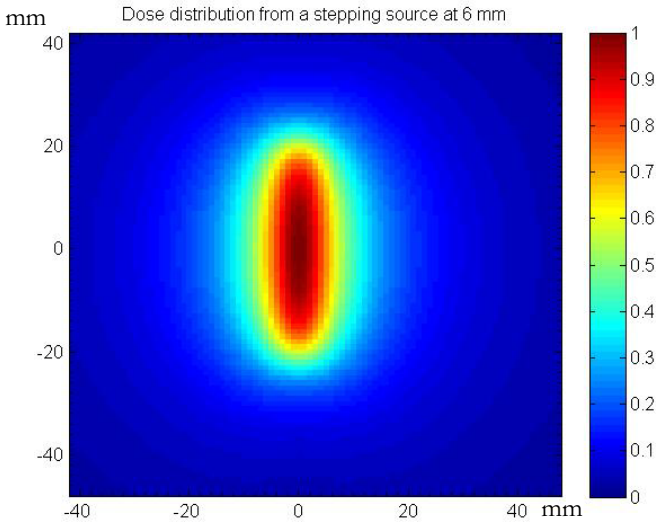

Figure 19: *Dose distribution from PLATO file export using RW-4.*

It is no longer possible to see the dose from the source dwell positions in the images, due to the increased distance between the needle and measuring point. The dose distributions now looks almost the same for both step lengths which indicates that there are only minimal difference between plans using either 2.5 mm or 5 mm step length (figure 38-40 in the appendix section).

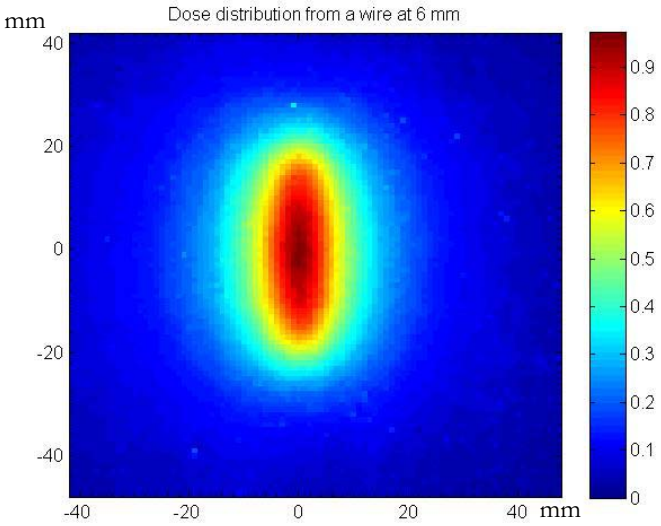

Figure 20: *Dose distribution from the wire measurement.*

The dose distribution from the wire at 6 mm distance is shown in figure 20. The 20-40% isodoses of D_{max} stretches further out than it does for the plans

made by the TPS. However, the difference looks small for the naked eye. The 95% isodose is for the wire measurement still relatively smaller than for the PLATO plans.

The percental difference (figure 21 and 22) shows that there is a smaller difference in dose distribution within the clinically relevant area than it is longer out from the source. The difference for RW-2 is ±10% while it is ±20% for RW-4. The clinically relevant area does not stretch further out than 10 mm from the wire or needle.

The same trend can still be seen at 6 mm distance as it was for 1 mm distance, that there is a larger difference between the ends and the center of the needle.

Since both plan images looks the same, both the percental images will look alike. It is however, possible to see some difference in the dose distribution especially at the ends of the source. There is a better agreement for the 6 mm distance because of the increased evaluation distance.

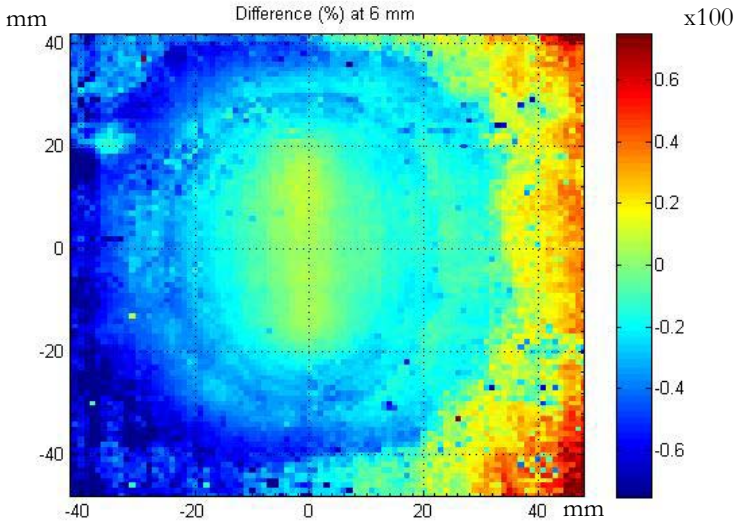

Figure 21: *The percental difference in dose distribution between the PLATO plan and the wire measurement using RW-2.*

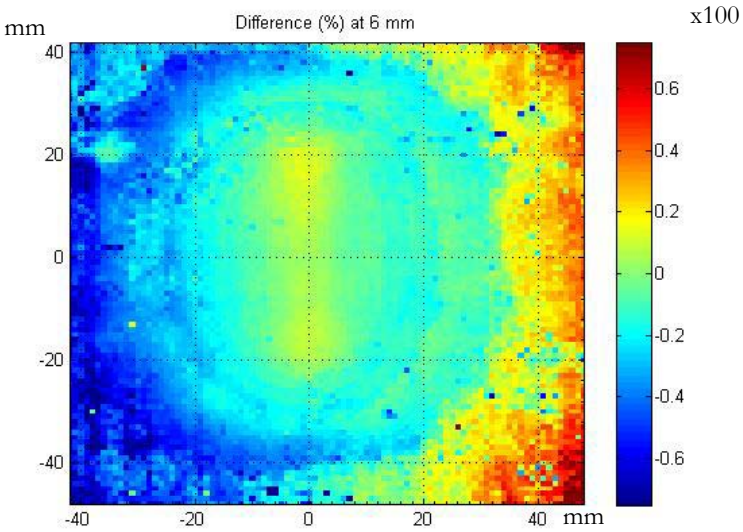

Figure 22: *The percental difference in dose distribution between the PLATO plan and the wire measurement using RW-4.*

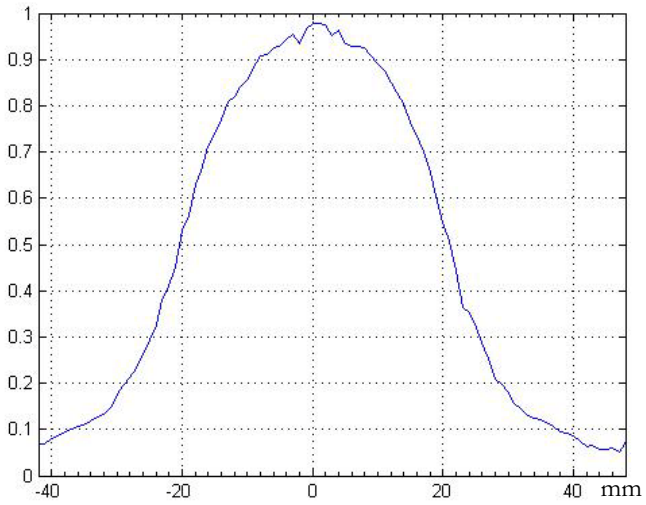

Figure 23: *Shows a plot of the dose distribution from the wire measurement. Plotted values originate straight through the wire at 6 mm distance.*

Figure 23 shows a plot of the dose distribution from the wire measurement at 6 mm distance between the source and the film.

When using RW-1 (figure 24), which has a smaller EL than RW-2, the same trend still occurs. Compare figures 21 and 24.

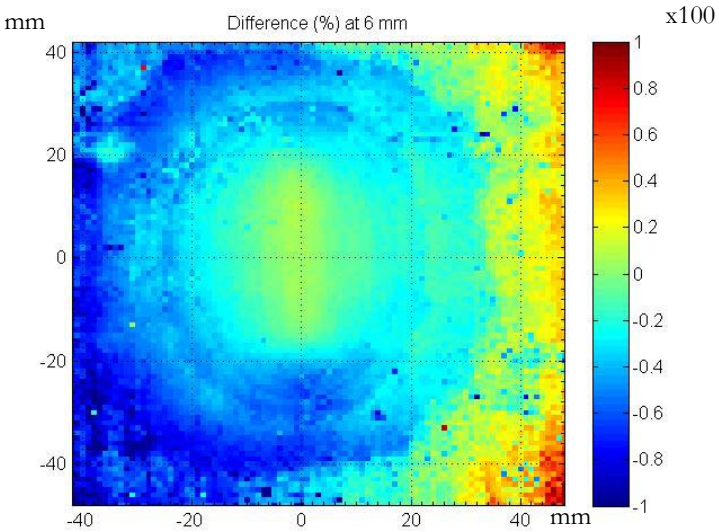

Figure 24: *The percental difference in dose distribution between the PLATO plan and the wire measurement using RW-1.*

11 mm Distance

The first three figures (figure 25-27) only show, as in the previous sections, the results before they are compared using MATLAB®. Figure 25 is the PLATO file export using 2.5 mm step length, figure 26 is PLATO file export using 5.0 mm step length and figure 27 show the wire measurement. All values are normalized to the highest dose value in each image throughout this section.

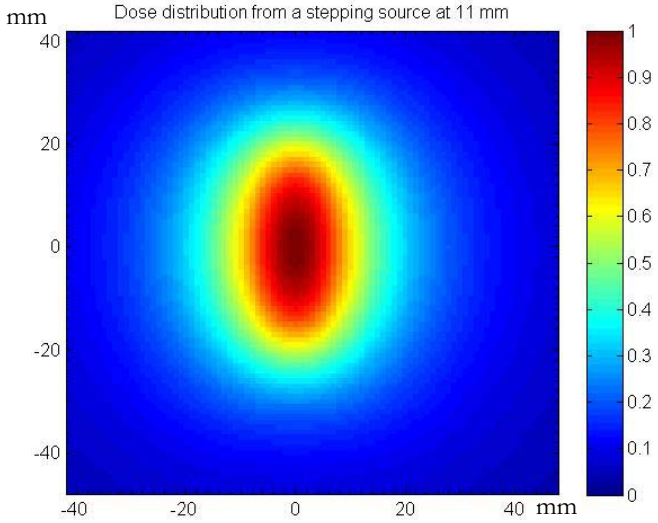

Figure 25: *Dose distribution from PLATO file export using RW-2.*

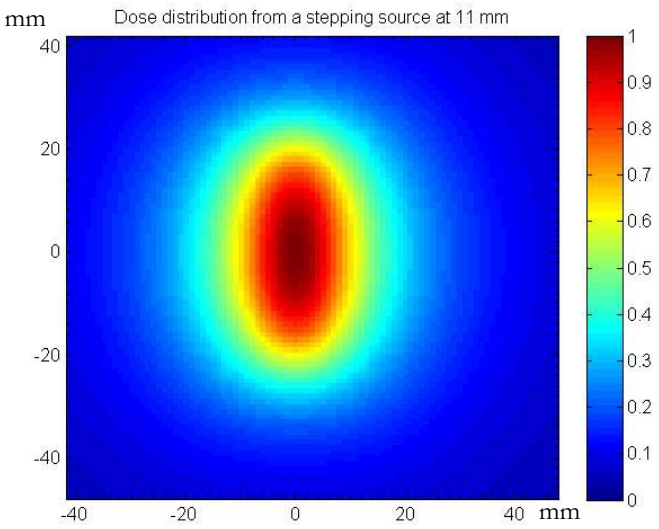

Figure 26: *Dose distribution from PLATO file export using RW-4*

The dose distributions still look almost the same for both step lengths. The 95% isodose now extends relatively far out, close to the margin of the clinically relevant area.

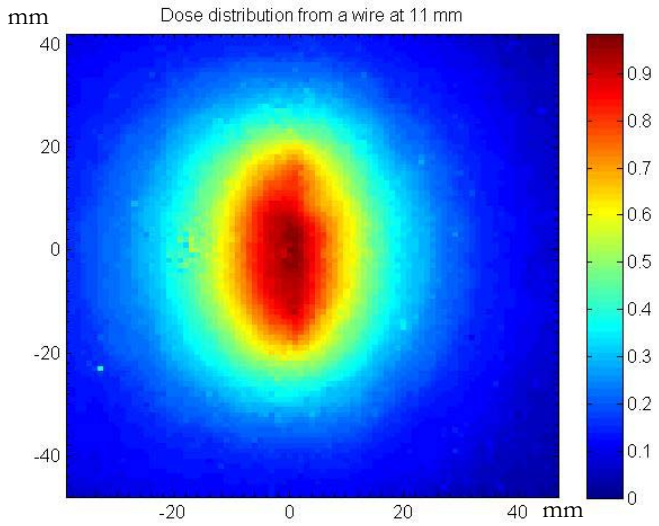

Figure 27: *Dose distribution from the wire measurement.*

The dose distribution from the wire at 11 mm distance is shown in figure 27. The light blue part stretches further out than it does for the plans made by the TPS, the differences however, looks small. The 95% isodose is for the wire measurement still relatively smaller than for the PLATO plans as it should be.

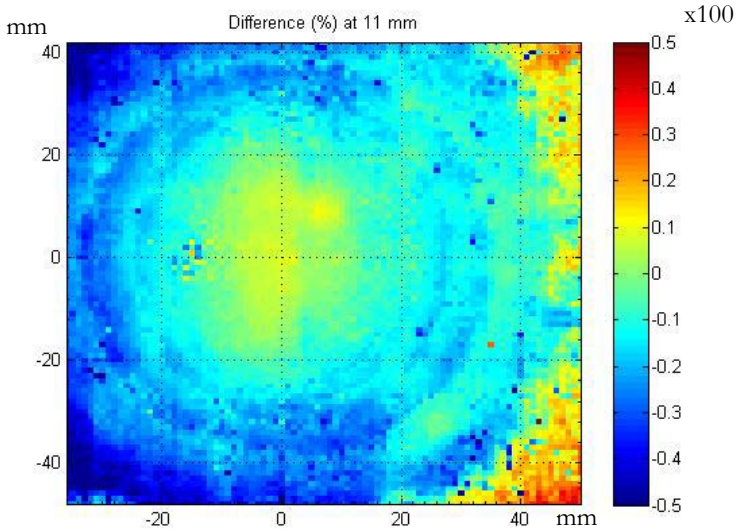

Figure 28: *The percental difference in dose distribution between the PLATO plan and the wire measurement using RW-2.*

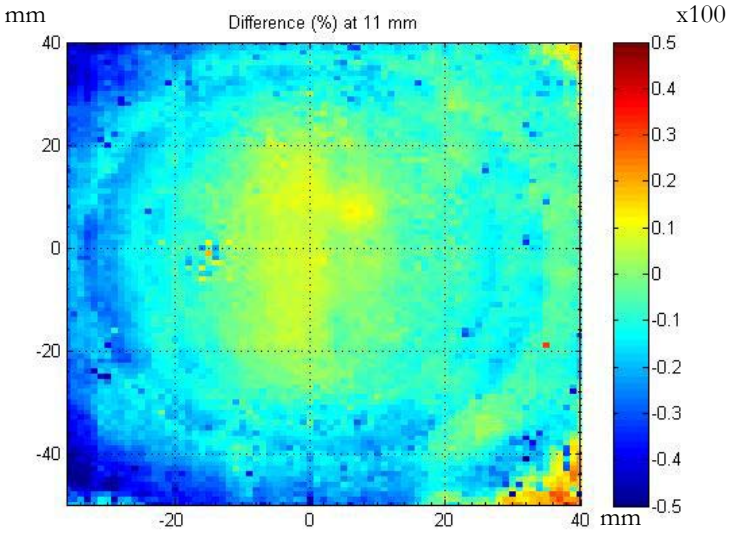

Figure 29: *The percental difference in dose distribution between the PLATO plan and the wire measurement using RW-4.*

The percental difference images (figure 28 and 29) no longer show any clear results within the clinically relevant area. The clinically relevant area does not stretch further out than 10 mm from the wire or needle. The difference in dose distribution is now too smeared out to give any conclusive results for both 2.5 mm and 5.0 mm step lengths. It is however, less than 15%.

A trend that is possible to see, is visible if one looks at the colorbar in the percental difference images (figures 14-15 and 17, 21-22 and 24, 28-29 and 31) that the maximum value on that bar changes and is getting reduced with the increased distance between the wire and the film. This means that longer dis-

tance between source and point of interest gives less difference in dose distribution between PLATO plan and wire measurement. However, within the clinically relevant area the differences are too significant to neglect.

Figure 30 shows a plot of the values from the wire measurement at 11 mm distance.

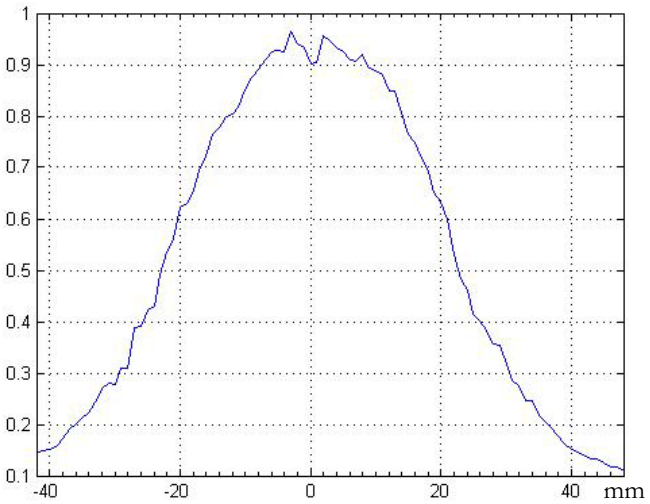

Figure 30: *Shows Shows a plot of the dose distribution from the wire measurement. Plotted values originate straight through the wire at 11 mm distance.*

When using RW-1 (figure 31), which has a smaller EL than RW-2, the same trend still occurs. Compare figures 28 and 31.

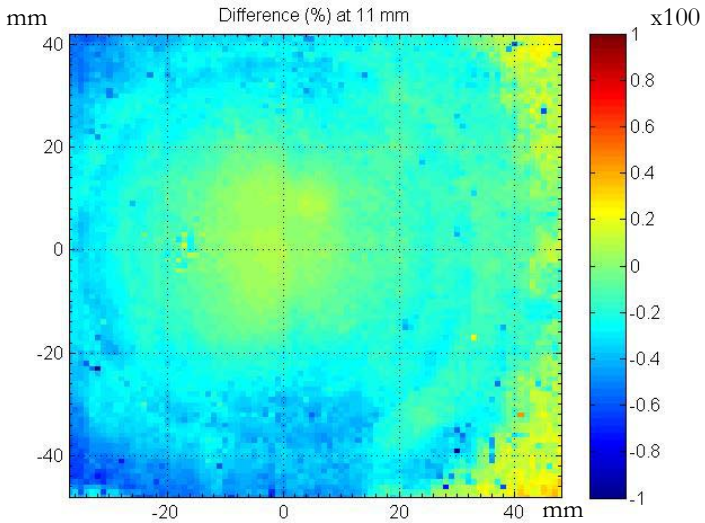

Figure 31: *The percental difference in dose distribution between the PLATO plan and the wire measurement using RW-1.*

Dose Difference and Variation

A total of six different RWs were used (table 2), which means that there will be a dose difference between each of the RWs and the wire measurements. A ratio between the dose values in the calculated PLATO plans and the wire measurements is calculated using Eq. 12.

$$Ratio = \frac{D_{PLATO}}{D_{Wire}} \tag{12}$$

The ratio is presented in tables for both different distances from the source (table 5-6) and for different distances from the plane center (table 12-14). Figure 45 in the appendix section show where the points are in relation to the source.

Table 5: *The ratio between the dose values in both the calculated PLATO plan and the wire measurements for the 1 mm plane. The ratio is presented at different distances from the sources center.*

	2 mm	3 mm	4 mm	5 mm	6 mm	7 mm	8 mm	9 mm	10 mm
RW-1	0.992	0.902	0.867	0.858	0.815	0.761	0.779	0.766	0.707
RW-2	0.992	0.907	0.873	0.866	0.825	0.773	0.792	0.781	0.723
RW-3	0.885	0.771	0.732	0.722	0.685	0.640	0.655	0.644	0.594
RW-4	0.749	0.743	0.733	0.734	0.702	0.659	0.678	0.671	0.622
RW-5	0.776	0.618	0.557	0.535	0.503	0.468	0.479	0.472	0.437
RW-6	0.220	0.292	0.335	0.363	0.363	0.350	0.364	0.363	0.338

Table 6: *The ratio between the dose values in both the calculated PLATO plan and the wire measurements for the 6 mm plane. The ratio is presented at different distances from the sources center.*

	7 mm	8 mm	9 mm	10 mm
RW-1	1.012	0.993	0.972	0.917
RW-2	1.015	0.995	0.979	0.926
RW-3	1.012	0.993	0.972	0.916
RW-4	1.018	1.005	0.988	0.936
RW-5	1.009	0.990	0.971	0.917
RW-6	0.947	0.947	0.939	0.894

Correction of Dwell Weights

Figures 16, 23 and 30 show a plot of the values from the wire measurement at 1 mm, 6 mm and 11 mm distance respectively. The values are the ones in the column of the dose matrix that run through the entire length of the wire. A dose profile along the midplane shown as a plot of the whole dose matrix

would display all isodose curves and making it impossible to read out more than the first few with the highest values.

Since the step lengths and position of the wire in the plots are known, a preliminary correction was made by finding each dwell position in the plot and correcting it after that specific value. The wires position is between -18 mm and 18 mm with its center at 0 mm, giving it a total length of 36 mm.

1 mm Distance

The percental difference between PLATO plan and wire measurement after the dwell weight correction for both 2.5 mm and 5.0 step lengths (figure 32 and 33).

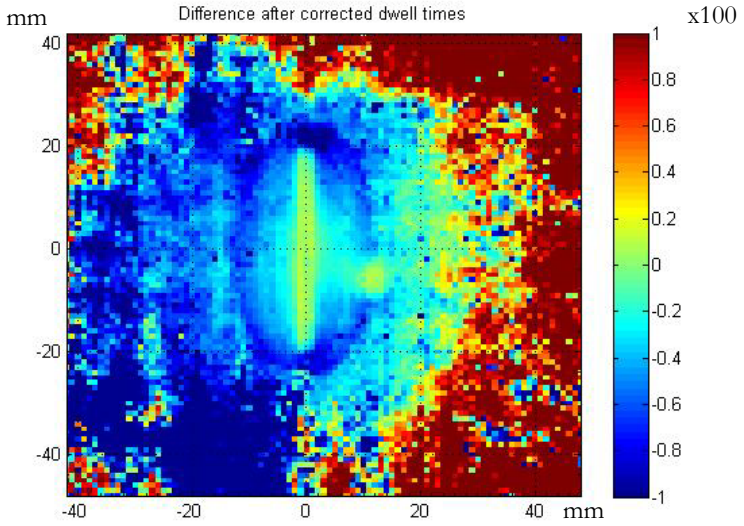

Figure 32: *The percental difference in dose distribution between the PLATO plan and the wire measurement after the dwell weight correction using RW-2.*

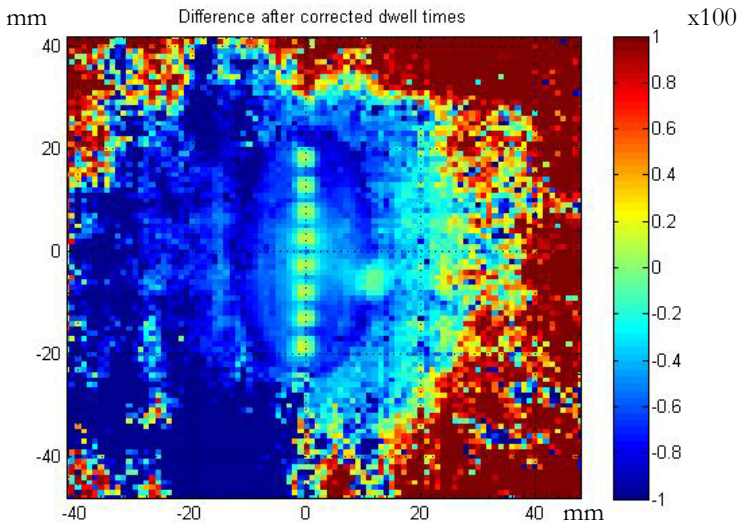

Figure 33: *The percental difference in dose distribution between the PLATO plan and the wire measurement after the dwell weight correction using RW-4.*

The trend with larger differences at the ends are now gone, and it is possible to see that there is a better agreement between plan and measurement very close to and within the needle. There is however, a worse agreement in dose distribution further out. To get better agreements on other locations, another curve needs to be used.

The decision of choosing the interesting areas lies solely in the hands of the physicians, in terms of how they would like the results presented and which parts they want enhanced. Since no interesting area yet has been chosen, these are merely preliminary results.

6 mm Distance

The percental difference between PLATO plan and wire measurement after the dwell weight correction for both 2.5 mm and 5.0 step lengths (figure 34 and 35).

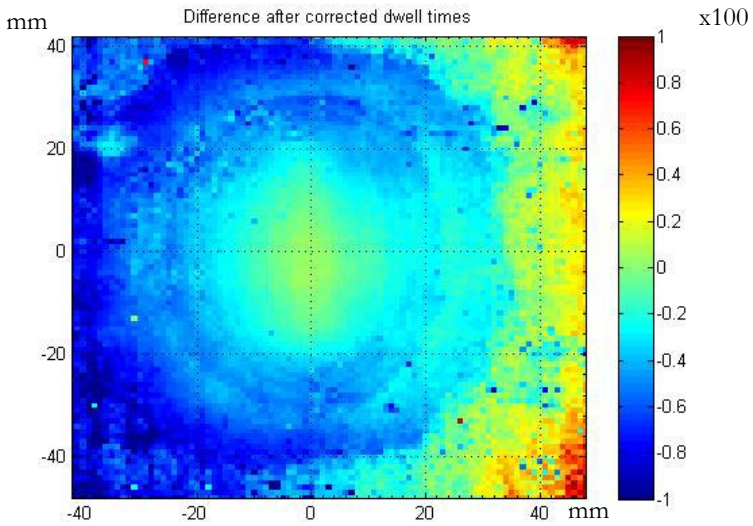

Figure 34: *The percental difference in dose distribution between the PLATO plan and the wire measurement after the dwell weight correction using RW-2.*

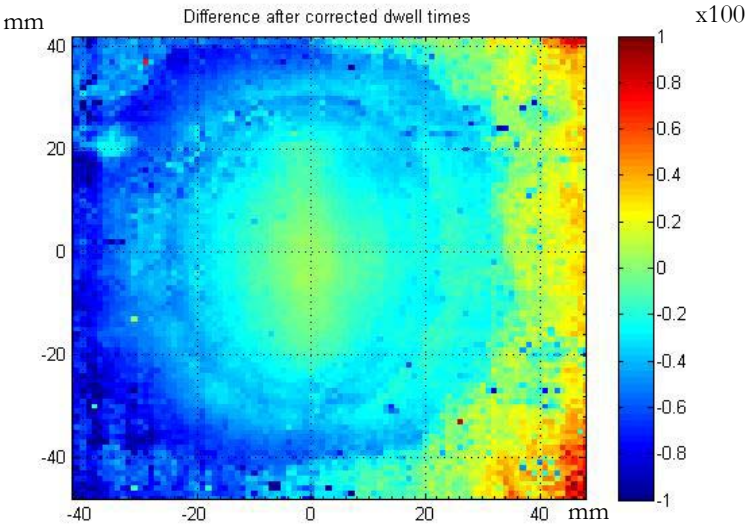

Figure 35: *The percental difference in dose distribution between the PLATO plan and the wire measurement after the dwell weight correction using RW-4.*

The trend with a larger difference at the ends is still gone, and it is possible to see that there is a better agreement between plan and measurement very close to and within the needle. There is still a worse agreement in dose distribution further out. To get better agreements on other locations, same as before applies; other curves need to be used.

11 mm Distance

The percental difference between PLATO plan and wire measurement after the dwell weight correction for both 2.5 mm and 5.0 step lengths (figure 36 and 37).

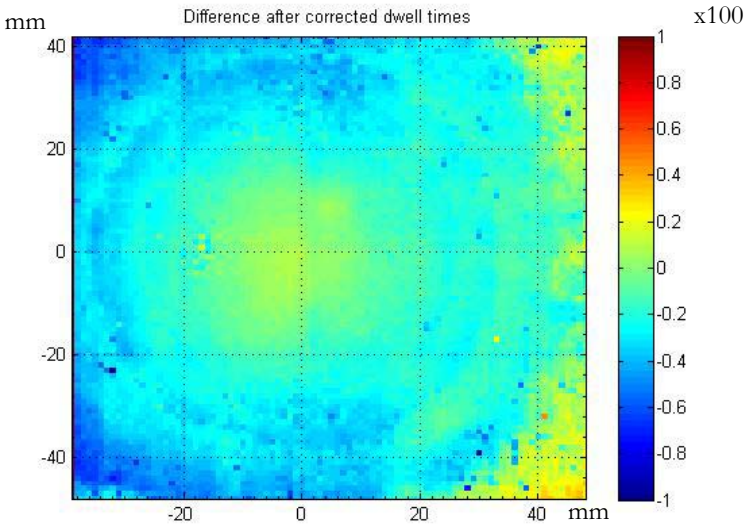

Figure 36: *The percental difference in dose distribution between the PLATO plan and the wire measurement after the dwell weight correction using RW-2.*

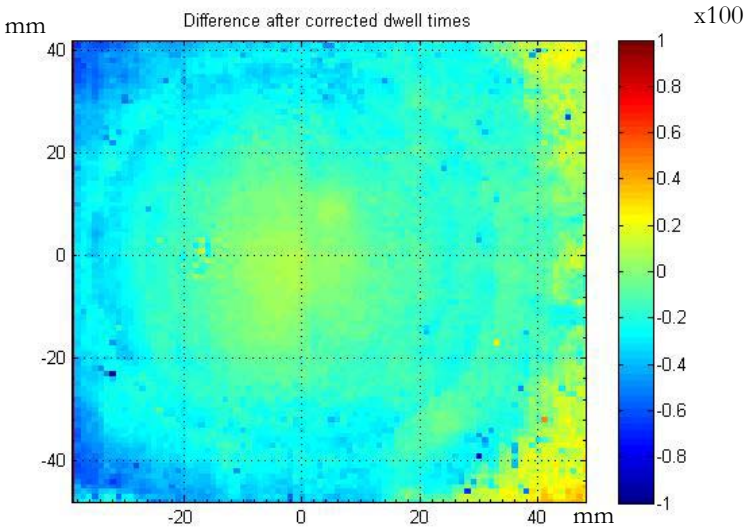

Figure 37: *The percental difference in dose distribution between the PLATO plan and the wire measurement after the dwell weight correction using RW-4.*

The percental difference images (figure 36 and 37) no longer show any clear results within the clinically relevant area. The difference in dose distribution is

too smeared out to give any conclusive results for both 2.5 mm and 5.0 mm step lengths.

Conclusions

The differences between NPS and PLATO are because of several reasons. One obvious is due to the difference in EL of the RW. This leads to that there will be larger differences further away from the center. At the ends the wire has lower dose rate than in the center while the stepping source still has the same. Another reason to the differences is due to approximations made by NPS, which are insufficient in capturing the change in source specific attenuation properties. Source specific calculation gives larger doses, which means that NPS underestimates the treated volume for larger angles. The differences in calculation algorithms have however, only a minor impact in the difference in dose distribution.

There is general under dosage outside the catheter and cold spots between source positions for longer step lengths close to the source. There are however, hot spots at the actual source positions for longer step lengths. For shorter step lengths there is an even dose distribution close to the centre.

Results from the ratio between dose values support the initial comparisons. The results show a better compliance close to the source, which indicates that there is a large angular dependence.

The differences in dose distribution are mainly due to that the AL is not the same as the EL. Another reason is that equal dwell weights were used initially. The difference in distance from the source will also have impact on the results; there is a better agreement closer to the source.

It is clear that corrections of the dwell weights have to be made to correct for the difference of the stepping source to emulate the dose distribution from the wire. Using dose matrix values from within the source position, it is possible to get better agreement only close to the source. Further away from the source results, in this case, in worse agreement. This indicates that dose matrix values at a certain distance from the source must be used to get a better agreement at that specific distance.

Acknowledgements

I would like to end with expressing my gratitude to my supervisor Jens M. Edmund for his dedication and continuous support.

I would also like to thank "Regementsläkaren Dr. Hartelii stipendiestiftelse" and "Stiftelsen skåneföreningen 1900-års mäns stipendiefond" for funding an extension of this work as well as "John och Augusta Persons stiftelse" for funding a presentation of this work at ESTRO 29.

Great appreciations to the hospital physicists at Herlev hospital for all the help you have given me.

Finally, I would like to express my gratitude to my fellow students for valuable and helpful input as well as rewarding discussions.

Lund, June 16 2010

Daniel Gasic

Bibliography

1. Erickson, B. and Wilson, J.F., "*Clinical indications for brachytherapy."* J. Sur. Oncol., Vol. **65**, pp. 218-227, 1997.

2. Harrison, L.B.*, "Applications of brachytherapy in head and neck cancer."* Semin. Surg. Oncol., Vol. **13**, pp. 177-184, 1997.

3. Cerezo, L.; Liu, F.-F.; Tsang, R. and Payne, D., "*Squamous cell carcinoma of the lip: analysis of the Princess Margaret Hospital experience."* Radiother. Oncol., Vol. **28**, pp. 142-147, 1993.

4. Byers, R.M.; O'Brien, J. and Waxler, J., "*The therapeutical and prognostic implications of nerve invasion in cancer of the lower lip."* Int. J. Radiat. Oncol. Biol. Phys., Vol. **4**, pp. 215-217, 1978.

5. Cowen, D.; Thomas, L.; Richaud, P.; Pierre, F. and Pigneux, J., "*Cancer of the lips: Results of the treatment of 299 patients."* Ann. Otol. Chir. Cervicofacial, Vol. **107**, pp. 121-125, 2, 1990.

6. Petrovich, Z.; Kuisk, H.; Tobochnick, N.; Little, R.E.; Barton, R. and Jose, L., "*Carcinoma of the lip."* Arch. Otolaryngol., Vol. **105**, pp. 187-191, 1979.

7. Fitzpatrick, P.J., "*Cancer of the lip."* J. Otolaryngol, Vol. **13**, pp. 32-36, 1, 1984.

8. Baker, S.R. and Krause, C.J., "*Carcinoma of the lip."* The Laryngoscope, Vol. **90**, pp. 19-27, 1980.

9. De Visscher, J.G.A.M.; Grond, A.J.K.; Botke, G. and van der Waal, I., "*Results of radiotherapy for squamous cell carcinoma of the vermillion border of the lower lip. A retrospective analysis of 108 patients."* Radiother. Oncol., Vol. **39**, pp. 9-14, 1996.

10. Pigneux, J.; Richaud, P. and Lagarde, C., "*The place of interstitial therapy using ^{192}Iridium in the management of carcinoma of the lip."* Cancer, Vol. **43**, pp. 1073-1077, 1979.

11. *AAPM Report No. 51, Report of the AAPM radiation therapy committee Task Group 43: Dosimetry of Interstitial Brachytherapy Sources.* 1995.

12. *Update of AAPM Task Group No. 43 report: A revised AAPM protocol for brachytherapy dose calculations.* 2004.

13. Nath, R.; Anderson, L.L.; Luxton, G.; Weaver, K.A.; Williamson, J.F. and Meigooni, A.S., "*Dosimetry of interstitial brachytherapy sources: Recommendations of the AAPM Radiation Therapy Committee Task Group No. 43."* Med. Phys., Vol. **22**, pp. 209-234, 1995.

14. Anderson, L.L; Nath, R.; Weaver, K.A.; Nori, D.; Phillips, T.L.; Son, Y.H.; Chiu-Tsao, S.-T.; Meigooni, A.S.; Meli, J.A. and Smith, V., "*Interstitial Collaborative Working Group (ICWG).*" Raven, New York : s.n., 1990, Interstitial Brachytherapy: Physical, Biological and Clinical Considerations.

15. Weaver, K.A.; Smith, V.; Huang, D.; Barnett, C.; Schell, M.C. and Ling, C., "*Dose parameters of ^{125}I and ^{192}Ir seed sources.*" Med. Phys., Vol. **16**, pp. 636-643, 4, 1989.

16. Nath, R.; Meigooni, A.S. and Meli, J.A., "*Dosimetry on the transverse axis of ^{125}I and ^{192}Ir interstitial brachytherapy sources.*" Med. Phys., Vol. **17**, pp. 1032-1040, 6, 1990.

17. Williamson, J.F. and Zuofeng, L., "*Monte Carlo aided dosimetry of the microselectron pulsed and high dose-rate ^{192}Ir sources.*" Med. Phys., Vol. **22**, pp. 809-819, 6, 1995.

18. *AAPM Report No. 21, Report of the AAPM radiation therapy committee Task Group 32: Specification of brachytherapy source strength.* American Institute of Physics, New York : s.n., 1987.

19. *ICRU 38, Dose and Volume Specification for Reporting Intracavitary Therapy in Gynecology.* s.l. : International Commission on Radiation Units and Measurements, Bethesda, MD, 1985.

20. *ICRU 60, Fundamental Quantities and Units for Ionizing Radiation.* s.l. : International Commission on Radiation Units and Measurements, Bethesda, MD, 1998.

21. Podgorsak, E.B., "*Radiation Oncology Physics: A Handbook for Teachers and Students.*" Vienna : International Atomic Energy Agency (IAEA), 2005.

22. Meisberger, L.L.; Keller, R. and Shalek, R.J., "*The effective attenuation in water of gamma rays of gold-198, iridium-192, cesium-137, radium-226 and cobalt-60.*" Radiology, Vol. **90**, pp. 953-957, 1968

23. Bice Jr, W.S.; Prestidge, B.R.; Prete, J.J. and Dubois, D.F., "*Clinical Impact of Implementing the Recommendations of AAPM Task Group 43 on Permanent Prostate Brachytherapy Using ^{125}I.*" Int. J. Radiat. Oncol. Biol. Phys., Vol. **40**, pp. 1237-1241, 5, 1998.

24. Williamson, J.F., "*The accuracy of the line and point source approximations in Ir-192 dosimetry.*" Int. J. Radiat. Oncol. Biol. Phys., Vol. **12**, pp. 409-414, 3, 1986.

25. Han, Y.; Chu, S.S.; Huh, S.J. and Suh, C.-O., "*Independent Verification Program for High-Dose-Rate Brachytherapy Treatment Plans.*" J. Korean Soc. Ther. Radiol. Oncol., Vol. **21**, pp. 238-244, 3, 2003.

26. Wang, R. and Sloboda, R.S., "*Monte Carlo dosimetry of the VariSource high dose rate ^{192}Ir source."* Med. Phys., Vol. **25**, pp. 415-423, 4, 1998.

27. van der Laarse, R., *"Treatment Planning of Interstitial Radiotherapy (MPS) with the Selectron Treatment Planning System." In: Brachytherapy 1984.* Innsbruck : s.n., 1984. Proceedings 3rd International Selectron Users Meeting. pp. 286-294.

28. van Kleffens, H.J. and Star, W.M., "*Application of stereo x-ray photogrammetry (SRM) in the determination of absorbed dose values during intracavitary radiation therapy."* Int. J. Radiat. Oncol. Biol. Phys., Vol. **5**, pp. 557-563, 1979

29. Kuipers, F.; van der Laarse, R. and Minderhoud, T.J., "*Nucletron Planning System BPS user manual."* 1989.

30. Rustgi, S.N., "*Application of a diamond detector to brachytherapy dosimetry."* Phys. Med. Biol., Vol. **43**, pp. 2085-2094, 1998.

31. Perez, C.A. and Brady, L.W., "*Perez and Brady's Principle and practice of Radiation Oncology."* 5th. Philadelphia : Lippincott Williams & Wilkins, 2007.

32. Dries, W.J.F., "*Monte Carlo calculated dose distribution for endovascular HDR brachytherapy with Ir-192."* Radoitherapy and Oncology, Vol. **45**, pp. 77-82, 1997.

33. Gillin, M.T.; Albano, K.S. and Erickson, B., "*Planar and volume temporary interstitial implants: The Paris and other systems." In: Modern clinical brachytherapy physics.* [ed.] J.F. Williamson and R. and Thomadsen, B. Nath. Madison, WI : s.n., 1995, Med. Phys.

34. Dutreix, A., "*Can we compare systems for interstitial therapy?"* Radiother. Oncol., Vol. **13**, pp. 127-135, 1988.

35. Pierquin, B.; Wilson, J.F. and Chassagne, D., "*Modern brachytherapy."* Paris : Masson Publishing USA, Inc., 1987.

36. Marinello, G.; Valero, M.; Leung, S. and Pierquin, B., "*Comparative dosimetry between iridium wires and seed ribbons."* Int. J. Radiat. Oncol. Biol. Phys., Vol. **11**, pp. 1733-1739, 1985.

37. Marinello, G.; Pierquin, B.; Grimard, L. and Barret, C., "*Dosimetry of intraluminal brachytherapy."* Radiother. Oncol., Vol. **23**, pp. 213-216, 1992.

38. Hensley, F.W., "*Physics of Pulsed Dose-Rate Brachytherapy."* Proceedings of the 22nd Annual EMBS International Conference . pp. 2305-2307, 2000.

39. Perez, C.A. and Brady, L.W., "*Perez and Brady's Principles and Practice of Radiation Oncology."* 3rd. s.l. : Lippincott Williams & Wilkins, 1998.

40. Berns, C.; Fritz, P.; Hensley, F.W. and Wannenmacher, M., "*Consequences of optimization in PDR brachytherapy: is a routine geometrical optimization recommendable?"* Int. J. Radiat. Oncol. Biol. Phys., Vol. **37**, pp. 1173-1180, 5, 1997.

41. Kneschaurek, P.; Schiessl, W. and Wehrmann, R., "*Volume-based dose optimization in brachytherapy."* Int. J. Radiat. Oncol. Biol. Phys., Vol. **45**, pp. 811-815, 3, 1999.

42. Major, T.; Polgár, C.; Fodor, J.; Somogyi, A. and Németh, G., "*Conformality and homogenity of dose distributions in interstitial implants at idealized target volumes: A comparison between the Paris and dose-point optimized systems."* Radiother. Oncol., Vol. **62**, pp. 103-111, 2002.

43. Major, T.; Polgár, C.; Fodor, J.; Takácsi-Nagy, Z.; Mangel, L. and Németh, G., "*Evaluation of geometrically optimized single- and double-plane interstitial high dose rate implants with respect to conformality and homogenity."* Acta. Oncol., Vol. **42**, pp. 15-21, 1, 2003.

44. Brenner, D.J. and Hall, E.J., "*Conditions for the equivalence of continuous to pulsed low dose rate brachytherapy."* Int. J. Radiat. Oncol. Biol. Phys., Vol. **20**, pp. 181-190, 1, 1991.

45. Sminia, P.; Schneider, C.J.; Koedooder, K.; van Tienhoven, G.; Blank, L.E.C.M. and González, D., "*Pulse Frequency in pulsed brachytherapy based on tissue repair kinetics."* Int. J. Radiat. Oncol. Biol. Phys., Vol. **41**, pp. 139-150, 1, 1998.

46. Koedooder, K.; Blank, L.; van der Grient, H.; Pieters, B. and Kipp, B., "*From continuous low dose rate to pulsed dose rate brachytherapy: The practical benefits (Abstract)."* Radiother. Oncol., Vol. **75**, p. S57, 2005.

47. van Eijkeren, M.; Thienpont, M.; Boterberg, T. and De Neve, W., "*Implementation, uptime and safety of a pulsed dose rate afterloading machine."* Int. J. Radiat. Oncol. Biol. Phys., Vol. **36**, pp. 1233-1237, 5, 1996.

48. Hall, E.J. and Brenner, D.J., "*Pulsed dose rate brachytherapy: Can we take advantage of the new technology?"* Int. J. Radiat. Oncol. Biol. Phys., Vol. **34**, pp. 511-512, 2, 1996.

49. Visser, A.G.; van den Aardweg, G.J.M.J. and Levendag, P.C., "*Pulsed dose rate and fractionated high dose rate brachytherapy: Choise of brachytherapy schedules to replace low dose rate treatments."* Int. J. Radiat. Onco. Biol. Phys., Vol. **34**, pp. 497-505, 2, 1996.

50. McJury, M.; Tapper, P.D.; Cosgrove, V.P.; Murphy, P.S.; Griffin, S.; Leach, M.O.; Webb, S. and Oldham, M., "*Experimental 3D dosimetry around a high-dose-rate clinical ^{192}Ir source using a polyacrylamide gel (PAG) dosimeter."* Phys. Med. Biol., Vol. **44**, pp. 2431-2444, 1999.

51. Mazeron, J.-J.; Simon, J.M.; Le Pechoux, C.; Crook, J.M.; Grimard, L.; Piedbios, P.; Le Bourgeois, J.P. and Perquin, B., "*Effect of dose rate on local control anc complications in definitive irradiation of T1-2 squamous cell carcinomas of mobile tongue and floor of mouth with interstitial iridium-192.*" Radiother. Oncol., Vol. **21**, pp. 39-47, 1, 1991.

52. Peiffert, D.; Castelain, B.; Thomas, L.; Ardiet, J.-M.; Baillet, F. and Mazeron, J.-J., "*Pulsed dose rate brachytherapy in head and neck cancers. Feasibility study of a French cooperative group.*" Radiother. Oncol., Vol. **58**, pp. 71-75, 1, 2001.

53. Ulutin, H.C.; Ash, D. and Dodwell, D., "*Brachytherapy Boost to the Tumour Bed in High Risk Patients After Limited Surgery for Breast Cancer.*" Clinical Oncology, Vol. **15**, pp. 156-159, 3, 2003.

54. Serkies, K.; Badzio, A.; Jerczek-Fossa, B.; Tarnawska, Z.; Nowak, R.; Szewczyk, P. and Jassem, J., "*Rectal doses in intracavitary brachytherapy of gynecological malignancies: comparison of two dosimetric methods.*" Radiother. Oncol., Vol. **58**, pp. 37-41, 1, 2001.

55. Sandhu, A.S.; Symonds, P.R.; Robertson, A.G.; Reed, N.S.; McNee, S.G. and Paul, J., "*Interstitial iridium-192 implantation combined with external radiotherapy in anal cancer: ten years experience.*" Int. J. Radiat. Oncol. Biol. Phys., Vol. **40**, pp. 575-581, 3, 1998.

56. Rowe, D.E.; Carroll, R.J. and Day, C.L., "*Prognostic factors for local recurrence, metastasis, and survival rates in squamous cell carcinoma of the skin, ear, and lip.*" Journal of the American Academy of Dermatology, Vol. **26**, pp. 976-990, 6, 1992.

57. de Vries, Steven., "*Physics and Algorithms Oncentra MasterPlan Appendix B - Dose Calculation Validation for Brachy Planning.*" s.l. : Nucletron B.V., 2009.

58. van der Laarse, R.; Granero, D.; Pérez-Calatayud, J.; Meigooni, A.S. and Ballester, F., "*Dosimetric characterization of Ir-192 LDR elongated sources.*" Med. Phys., Vol. **35**, pp. 1154-1161, 3, 2008.

59. Nutting, C.; Horlock, N.; A'Hern, R.; Searle, A.; Henk, J.M.; Rhys-Evans, P. and Harrington, K., "*Manually after-loaded Ir-192 low dose rate brachytherapy after subtotal excision and flap reconstruction of recurrent cervical lymphadenopathy from head and neck cancer.*" Radiother. Oncol., Vol. **80**, pp. 39-42, 2006.

60. Kline, R.W.; Guillin, M.T.; Grimm, D.F. and Niroomand-Rad, A., "*Computer dosimetry of ^{192}Ir wire.*" Med. Phys., Vol. **12**, pp. 634-638, 1985

61. Guillin, M.T.; López, F.; Kline, R.W.; Grimm, D.F. and Niroomand-Rad, A. "*Comparison of measured and calculated dose distribution around a ^{192}Ir wire.*" Med. Phys., Vol. **15**, pp. 915-918, 1988.

62. Chiu-Tsao, S.-T.; Duckworth, T.L.; Patel, N.S.; Pisch, J. and Harrison, L.B., "*Verification of Ir-192 near source dosimetry using GAFCHROMIC film.*" Med. Phys., Vol. **31**, pp. 201-207, 2, 2004.

63. Daskalov, G.M.; Loffler, E. and Williamson, J.F., "*Monte Carlo-aided dosimetry of a new high dose-rate brachytherapy source.*" Med. Phys., Vol. **25**, pp. 2200-2208, 1998.

64. Lliso, F.; Pérez-Calatayud, J.; Carmona, V.; Ballester, F.; Lluch, J.L.; Serrano, M.A.; Limami, Y. and Casal, E., "*Fitted dosimteric parameters of high dose-rate 192Ir sources acording to the AAPM TG43 formalism.*" Med. Phys., Vol. **28**, pp. 654-660, 4, 2001.

65. Kajzer, W.; Krauze, A.; Walke, W. and Marciniak, J., "*Corrosion behaviour of AISI 316L steel in artificial body fluids.*" Journal of Achievements in Materials and Manufacturing Engineering, Vol. **31**, pp. 247-253, 2, 2008.

Appendix

Table 7: *The absorbed dose in cGy/h in water in the center-plane of ^{192}Ir wires with a diameter of 0.3 mm and normal linear air kerma rate of 1 $cGy*h^{-1}*m^2*cm^{-1}$ taking the slanted filtration of the radiation through the platinum casing and the absorption of the gamma rays in water into account. The upper bold values are the distances, in cm, between the source and the point of interest while the bold values on the left side are the wire length also in cm* [v].

	0.2	**0.3**	**0.4**	**0.5**	**0.6**	**0.7**	**0.8**	**0.9**	**1.0**	**1.1**	**1.2**
1	13.1	7.63	5.00	3.52	2.60	1.99	1.57	1.27	1.05	0.875	0.743
2	14.8	9.30	6.55	4.90	3.82	3.06	2.50	2.09	1.76	1.51	1.30
3	15.3	9.86	7.13	5.48	4.37	3.59	3.00	2.55	2.19	1.91	1.67
4	15.5	10.1	7.40	5.76	4.66	3.87	3.28	2.82	2.46	2.16	1.91
5	15.6	10.3	7.55	5.92	4.83	4.04	3.45	2.99	2.63	2.33	2.08
6	15.7	10.3	7.65	6.02	4.94	4.16	3.57	3.11	2.74	2.44	2.19
7	15.8	10.4	7.71	6.09	5.01	4.23	3.65	3.19	2.82	2.52	2.27
8	15.8	10.4	7.76	6.14	5.06	4.29	3.70	3.25	2.88	2.58	2.33
10	15.8	10.5	7.82	6.21	5.13	4.36	3.78	3.33	2.96	2.67	2.42
12	15.9	10.5	7.86	6.25	5.17	4.41	3.83	3.38	3.01	2.72	2.47
14	16.0	10.6	7.88	6.28	5.20	4.44	3.86	3.41	3.05	2.75	2.50

Table 8: *The absorbed dose in cGy/h in water in the center-plane of ^{192}Ir wires with a diameter of 0.3 mm and normal linear air kerma rate of 1 $cGy*h^{-1}*m^2*cm^{-1}$ taking the slanted filtration of the radiation through the platinum casing and the absorption of the gamma rays in water into account. The upper bold values are the distances, in cm, between the source and the point of interest while the bold values on the left side are the wire length also in cm* [v].

	1	**2**	**3**	**4**	**5**	**6**	**7**	**8**	**10**	**12**	**14**
1	1.05	0.278	0.125	0.070	0.045	0.031	0.022	0.017	0.010	0.007	0.004
2	1.76	0.523	0.242	0.138	0.088	0.061	0.044	0.033	0.020	0.013	0.008
3	2.19	0.725	0.348	0.202	0.130	0.090	0.066	0.050	0.030	0.020	0.012
4	2.46	0.882	0.441	0.260	0.170	0.118	0.087	0.066	0.040	0.026	0.016
5	2.63	1.003	0.520	0.313	0.206	0.145	0.107	0.081	0.049	0.033	0.020
6	2.74	1.096	0.587	0.360	0.240	0.170	0.126	0.096	0.059	0.039	0.023
7	2.82	1.170	0.642	0.401	0.271	0.194	0.144	0.110	0.068	0.045	0.027
8	2.88	1.228	0.689	0.437	0.299	0.215	0.161	0.124	0.076	0.051	0.031
10	2.96	1.312	0.762	0.496	0.347	0.253	0.191	0.148	0.093	0.063	0.038
12	3.01	1.368	0.814	0.542	0.385	0.285	0.218	0.170	0.108	0.074	0.045
14	3.05	1.408	0.853	0.577	0.415	0.311	0.240	0.189	0.122	0.084	0.052

[v] Data from Eckert & Ziegler BEBIG GmbH, Iridium-192 wires - instructions for use - Appendix.

Table 9: *Presents the results from a 36 mm long wire and needle at two different step lengths for the parallel midplane. The results shown are the difference in dose at equal lengths as well as the difference in length at equal isodoses for the eleven points of interest, at different angles from origo in the coordinate system.*

	RW-1		RW-3	
Θ	ΔDose (%)	ΔLength (mm)	ΔDose (%)	ΔLength (mm)
0	0.42	0.03	0.34	0.05
10	0.61	0.04	0.44	0.06
20	0.60	0.04	0.36	0.07
30	0.65	0.04	0.33	0.08
40	0.73	0.07	0.67	0.11
45	0.76	0.09	0.77	0.13
50	0.47	0.08	0.41	0.14
60	0.74	0.18	0.80	0.30
70	0.27	0.39	0.75	0.79
80	-1.97	0.90	-3.85	1.91
90	-17.26	0.97	-37.95	1.57

Table 10: *Presents the results from a 36 mm long wire and needle at two different step lengths for the perpendicular midplane. The results shown are the difference in dose at equal lengths as well as the difference in length at equal isodoses for the eleven points of interest, at different angles from origo in the coordinate system.*

	RW-1		RW-3	
Θ	ΔDose (%)	ΔLength (mm)	ΔDose (%)	ΔLength (mm)
0	0.42	0.03	0.34	0.05
10	0.70	0.04	0.63	0.06
20	0.29	0.02	0.22	0.03
30	0.48	0.03	0.41	0.04
40	0.40	0.04	0.33	0.05
45	0.56	0.05	0.48	0.06
50	0.54	0.05	0.46	0.06
60	0.48	0.03	0.41	0.04
70	0.56	0.04	0.49	0.06
80	0.49	0.03	0.42	0.05
90	0.42	0.03	0.34	0.05

Table 11: *Some mathematical models accounting for attenuation and multiple scattering in a medium surrounding a radioactive source.*

Meisberger Approximation (22)	$\frac{X_W}{X_A} = A + Br + Cr^2 + Dr^3$ X_W = Exposure in water. X_A = Exposure in air. r = Distance (in cm) from source to point of calculation. A, B, C, D = Zero, first, second and third order polynomialfitting coefficients.
Van Kleffens and star expression (28)	$S(d) = \frac{1 + \alpha \cdot d^2}{1 + \beta \cdot d^2}$ d = Distance (in cm) from source to point of calculation α, β = Second order coefficients

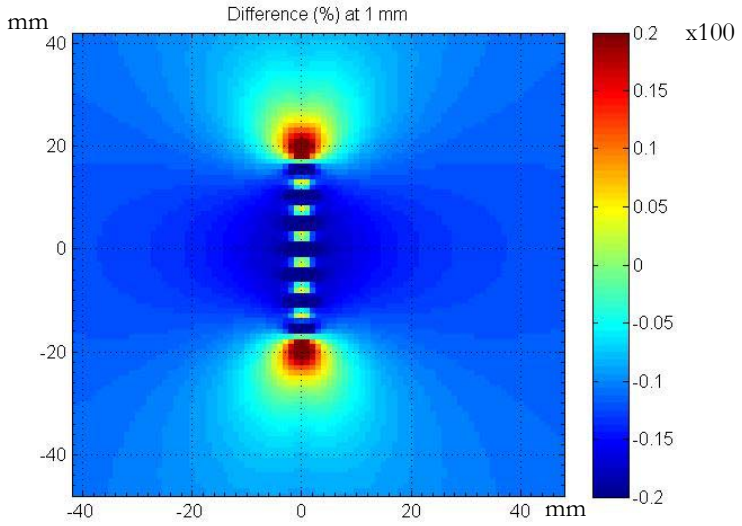

Figure 38: *The percental difference in dose distribution between two PLATO plans. The plans compared are equal in every way except the step length. In this image a plan using RW-4 is compared with a plan using RW-2 at the distance of 1 mm.*

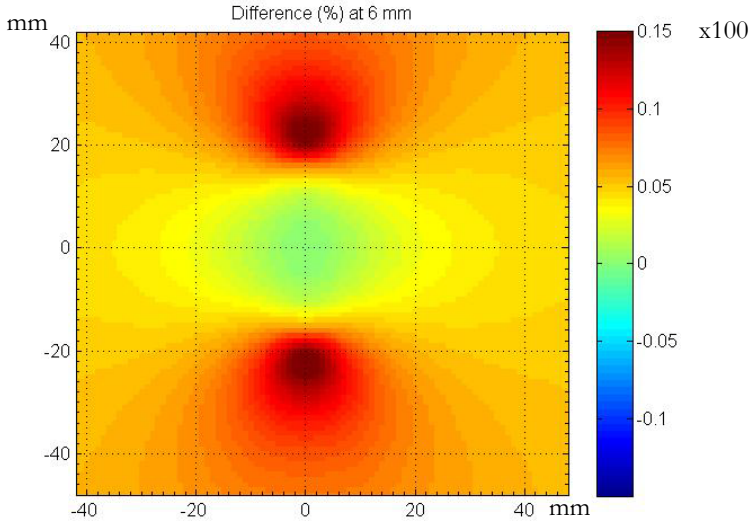

Figure 39: *The percental difference in dose distribution between two PLATO plans. The plans compared are equal in every way except the step length. In this image a plan using RW-4 is compared with a plan using RW-2 at the distance of 6 mm.*

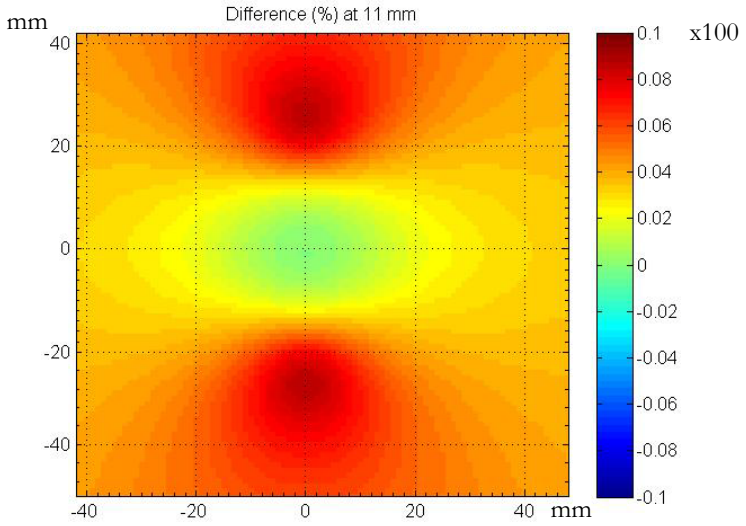

Figure 40: *The percental difference in dose distribution between two PLATO plans. The plans compared are equal in every way except the step length. In this image a plan using RW-4 is compared with a plan using RW-2 at the distance of 11 mm.*

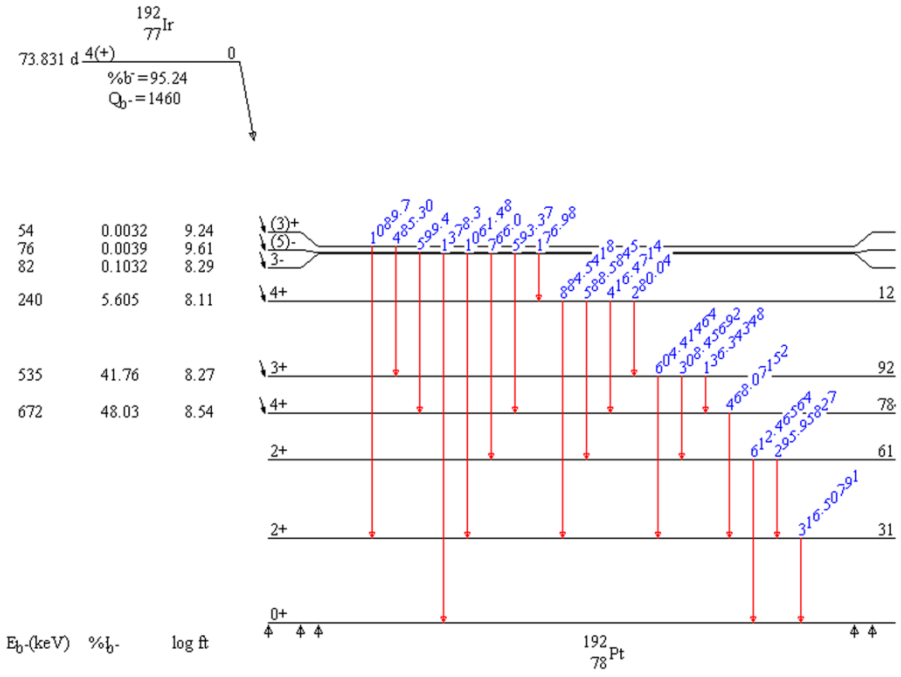

Figure 41: *The decay scheme for ^{192}Ir decaying to ^{192}Pt through β^- decay.*

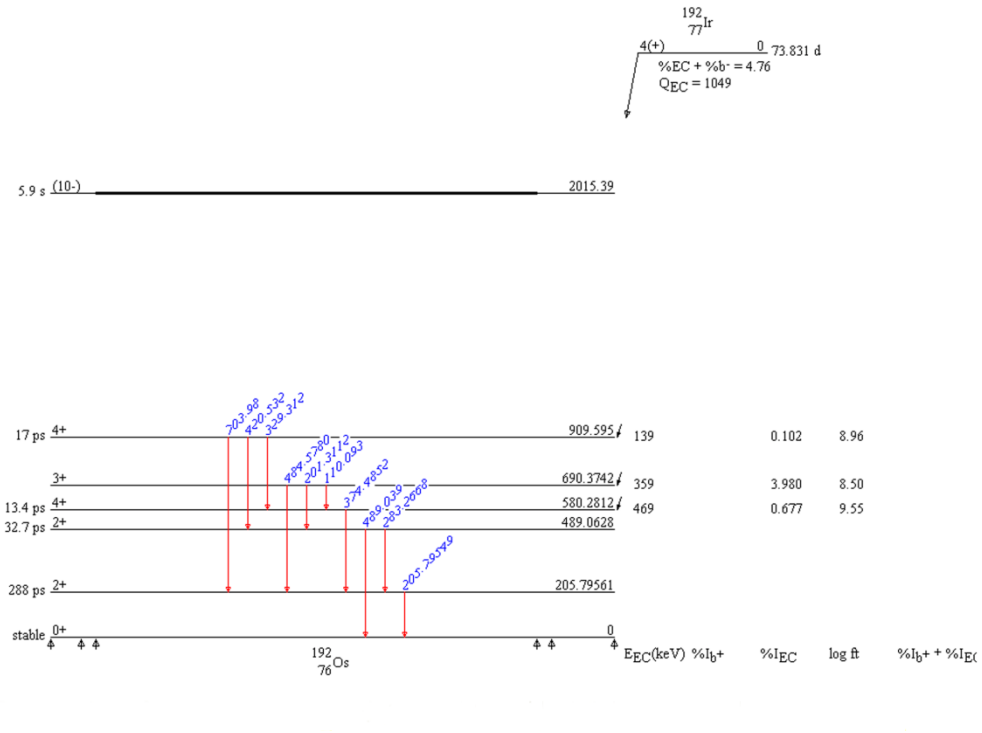

Figure 42: *The decay scheme for ^{192}Ir decaying to ^{192}Os through electron capture.*

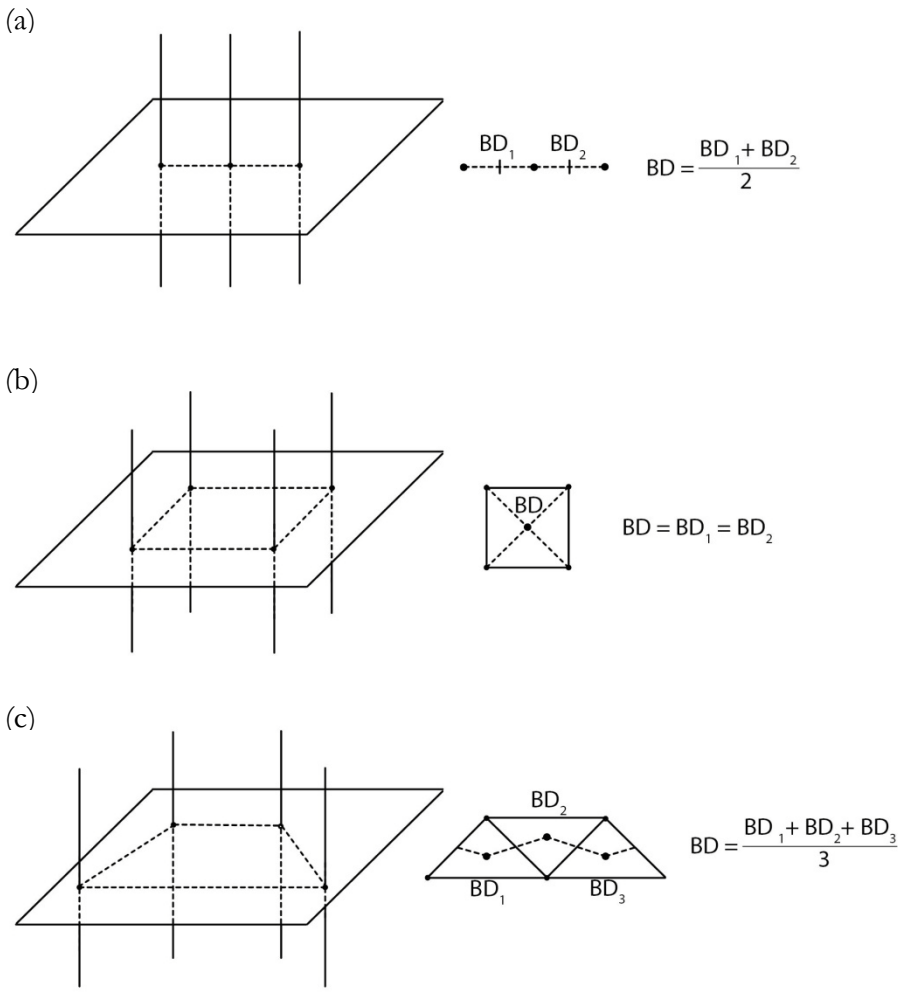

Figure 43: *In the Paris system, continuous radioactive lines of uniform linear activity (rectilinear sources) are arranged in one plane (a), in squares (b) or in triangles (c). In each of the above cases, the reference isodose is equal to 85% BD, which is the arithmetic mean of elementary BD calculated in the central plane.*

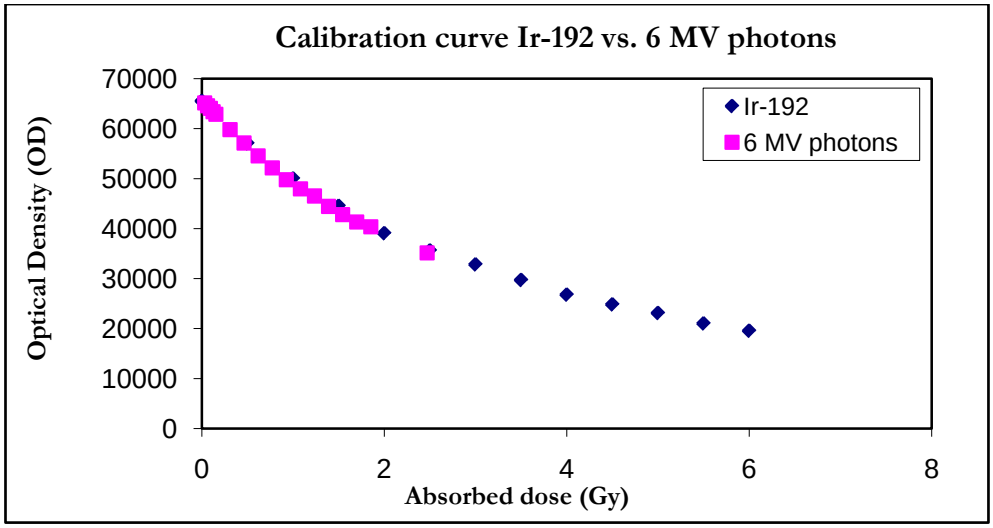

Figure 44: *Calibration curves from both the small ^{192}Ir stepping source and 6 MV photons from a Varian clinac 2300 iX.*

Table 12: *The ratio between the dose values in both the calculated PLATO plan and the wire measurements for the 1 mm plane. The ratio is presented at different distances from the plane center.*

	1 mm	2 mm	3 mm	4 mm	5 mm	6 mm	7 mm	8 mm	9 mm	10 mm
RW-1	1.223	1.053	0.892	0.864	0.858	0.812	0.758	0.781	0.765	0.704
RW-2	1.106	1.048	0.897	0.870	0.866	0.822	0.769	0.794	0.780	0.720
RW-3	1.060	0.834	0.759	0.728	0.722	0.683	0.637	0.656	0.643	0.592
RW-4	0.743	0.752	0.742	0.732	0.734	0.699	0.657	0.680	0.670	0.620
RW-5	1.012	0.715	0.601	0.551	0.534	0.501	0.466	0.480	0.472	0.435
RW-6	0.170	0.247	0.304	0.340	0.366	0.363	0.349	0.365	0.362	0.337

Table 13: *The ratio between the dose values in both the calculated PLATO plan and the wire measurements for the 6 mm plane. The ratio is presented at different distances from the plane center.*

	1 mm	2 mm	3 mm	4 mm	5 mm	6 mm	7 mm	8 mm	9 mm	10 mm
RW-1	1.022	1.033	1.026	1.005	0.995	0.984	0.967	0.917	0.905	0.901
RW-2	1.022	1.034	1.028	1.005	1.002	0.990	0.976	0.926	0.917	0.913
RW-3	1.021	1.032	1.026	1.004	0.997	0.983	0.967	0.916	0.904	0.899
RW-4	1.022	1.034	1.030	1.010	1.008	0.998	0.985	0.937	0.929	0.927
RW-5	1.020	1.031	1.022	1.000	0.995	0.981	0.966	0.917	0.907	0.904
RW-6	0.932	0.949	0.953	0.944	0.948	0.944	0.936	0.893	0.887	0.887

Table 14: *The ratio between the dose values in both the calculated PLATO plan and the wire measurements for the 11 mm plane. The ratio is presented at different distances from the plane center.*

	1 mm	2 mm	3 mm	4 mm	5 mm	6 mm	7 mm	8 mm	9 mm	10 mm
RW-1	1.087	1.091	1.085	1.068	1.064	1.047	1.057	1.062	1.020	1.010
RW-2	1.088	1.091	1.086	1.071	1.066	1.050	1.063	1.068	1.029	1.019
RW-3	1.088	1.092	1.087	1.072	1.068	1.054	1.067	1.074	1.035	1.028
RW-4	1.087	1.091	1.085	1.068	1.064	1.047	1.058	1.062	1.021	1.010
RW-5	1.088	1.091	1.086	1.071	1.066	1.052	1.063	1.068	1.029	1.019
RW-6	1.088	1.092	1.087	1.073	1.071	1.057	1.071	1.078	1.040	1.031

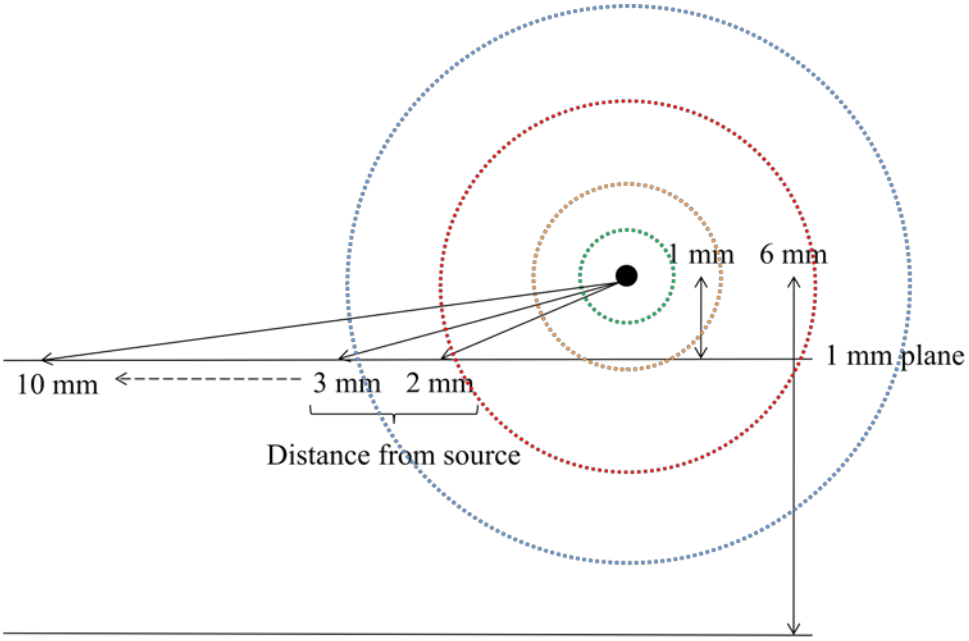

Figure 45: *The points are taken at a certain distance from the source which means that there will be lesser points for planes located longer away from the source since the last interesting value is located at the distance of 10 mm from the source.*